creative commons
COMMONS DEED

저작자표시-비영리-변경금지 2.0 대한민국

이용자는 아래의 조건을 따르는 경우에 한하여 자유롭게

- 이 저작물을 복제, 배포, 전송, 전시, 공연 및 방송할 수 있습니다.

다음과 같은 조건을 따라야 합니다:

저작자표시. 귀하는 원저작자를 표시하여야 합니다.

비영리. 귀하는 이 저작물을 영리 목적으로 이용할 수 없습니다.

변경금지. 귀하는 이 저작물을 개작, 변형 또는 가공할 수 없습니다.

- 귀하는, 이 저작물의 재이용이나 배포의 경우, 이 저작물에 적용된 이용허락조건을 명확하게 나타내어야 합니다.
- 저작권자로부터 별도의 허가를 받으면 이러한 조건들은 적용되지 않습니다.

저작권법에 따른 이용자의 권리는 위의 내용에 의하여 영향을 받지 않습니다.

이것은 이용허락규약(Legal Code)을 이해하기 쉽게 요약한 것입니다.

Disclaimer

dCollection

Master's Thesis
석사 학위논문

Pressure and Temperature Sensor with ZnO Nanowire Array

Kyung Hwa Lee (이 경 화 李 京 和)

Department of Information and Communication Engineering
정보통신융합공학전공

DGIST

2016

Master's Thesis
석사 학위논문

Pressure and Temperature Sensor with ZnO Nanowire Array

Kyung Hwa Lee (이 경 화 李 京 和)

Department of Information and Communication Engineering
정보통신융합공학전공

DGIST

2016

Pressure and Temperature Sensor with ZnO Nanowire Array

Advisor : Professor Jae Eun Jang

Co-advisor : Professor Seong-Woon Yu

by

Kyung Hwa Lee
Department of Information and Communication Engineering
DGIST

A thesis submitted to the faculty of DGIST in partial fulfillment of the requirements for the degree of Master of Science in the Department of Information and Communication Engineering. The study was conducted in accordance with Code of Research Ethics[1]

01. 08. 2016

Approved by

Professor Jae Eun Jang _____ (Signature)
(Advisor)

Professor Seong-Woon Yu _____ (Signature)
(Co-Advisor)

[1] Declaration of Ethical Conduct in Research**:** I, as a graduate student of DGIST, hereby declare that I have not committed any acts that may damage the credibility of my research. These include, but are not limited to: falsification, thesis written by someone else, distortion of research findings or plagiarism. I affirm that my thesis contains honest conclusions based on my own careful research under the guidance of my thesis advisor.

Pressure and Temperature Sensor with ZnO Nanowire Array

Kyung Hwa Lee

Accepted in partial fulfillment of the requirements for the degree of Master of Science.

01. 08. 2016

Head of Committee _____(인)
Prof. Jae Eun Jang

Committee Member _____(인)
Prof. Seong-Woon Yu

Committee Member _____(인)
Prof. Ji-Woong Choi

MS/IC
201422012

이 경 화. Kyung Hwa Lee. Pressure and Temperature Sensor with ZnO Nanowire Array, Department of Information and Communication Engineering. 2016. 49p. Advisor Prof. Jae Eun Jang, Co-Advisor Prof. Seong-Woon Yu.

ABSTRACT

Tactile sensors have recently attracted tremendous interest and the sensing mechanisms have been developed by mimicking the human touch system. However, most previous works have mostly focused on improving the sensitivity of sensors to physical parameters including pressure, strain or temperature. Also, achieving grip control of fragile objects such as eggs is main consideration in robotic hands development. For human beings, psychological feelings including softness, roughness and pain are important factors for interacting with others and the objects. If the tactile sensors which give psychological feelings are applied to various applications such as mobile displays, android robots and prosthetics, they have ability to sense psychological feelings as like humans. Among several emotions, ‘pain’ is the most important feeling because ‘pain’ is indication of damage and humans have self-protection ability by feeling ‘pain’ from external environment. Ultimately, robots with psychological tactile sensor will become as intelligent as human beings while robots perform the duties sensing danger and avoid it at the same time. In this way, realizing psychological tactile sensors is strongly required, however, mimicking psychological feelings is unprecedented until now. In order to perceive ‘pain’ feeling from harsh environments, tactile sensors need to detect pressure and temperature simultaneously. Here, we have demonstrated Zinc oxide nanowire based tactile sensors which can detect pressure and temperature simultaneously. Array type tactile sensors can verify the input objects which may be sharp, blunt, and hot or cool by simple signal processing. This capability means that tactile sensor can convey psychological feelings from the physical parameters. As a result, this tactile sensor can be used to protect android robot hand or mobile phone touch display from external risky environments.

Keywords: psychological tactile sensor, pain feeling, tactile sensing, ZnO nanowire array, pressure and temperature sensor

Contents

List of figures

I. **INTRODUCTION**

1.1 Overview

Humans have the ability to interact with the external environment through five main senses including vision, hearing, smell, taste and touch. The information perceived from the five senses is essential for human beings to lead a life. In particular, tactile sense plays a significant role in many aspects of life. The most basic human activities, such as grasping, and perceiving objects based on information such as their shape, size, temperature and texture, are possible thanks to the human tactile sensing system [1]-[3]. Furthermore, softness, roughness, smoothness and pain enrich human interaction with others and the objects. These psychological feelings are too important to be neglected in human lives. The 'pain' is one of the most important feelings among psychological feelings because it is indication of danger and the humans have self-protection ability by feeling 'pain' from external harsh environment.

Many research groups know the importance of tactile sensing in humanoids robots and other interfaces. Most of studies focused on detecting pressure and temperature in attempts to improve sensitivity of sensors or achieving grip control of robotic hands [4]-[8]. Unfortunately, mimicking psychological feelings including pain, softness, and roughness is unprecedented until now. As a result, the primary goal of this thesis is to realize 'pain' warning system by understanding the biomechanics of the human tactile system. Temperature and pressure can be the main physical parameters to define 'pain' feeling. Therefore, we devised one body tactile sensor which can detect pressure and temperature simultaneously with simple signal processing and this enables us to design tactile sensor with simple hardware.

1.2 Motivation

This research project will focus on setting up a ‘pain’ warning signal generation system. Understanding the mechanism of human tactile system is essential to realize tactile sensor for ‘pain’ perception. Many research regarding tactile sensors is performed but they are usually working on improving sensitivity of one modality sensor such as pressure, strain, temperature sensor [4]-[6]. Main issue for this project is to differentiate pressure and temperature sense which are physical variables for ‘pain’ feeling indication. Piezo-pyro electric nanowire is the main component of our tactile sensor and by utilizing Seebeck effect of free carriers in nanowires, detection and verifying two senses are realized.

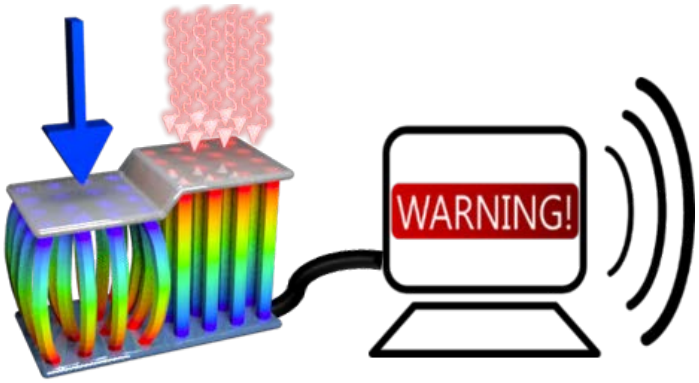

Fig 1.1 Schematic of ‘pain’ warning signal generation system. When the tactile sensor is under high pressure and temperature, ‘pain’ warning signal is generated.

There are many studies regarding the piezo-pyro electric materials for energy harvesting applications [9]-[13]. However, these works are only focused on improving efficiency of energy conversion and piezo-pyro electric output could not be differentiated by each other. This implies that one body tactile sensing from pressure and temperature variables is impossible so that the design and system become complicated when it comes to tactile sensing system with multi functions to be implemented in humanoid interfaces. In this way, this research project will emphasize the importance of developing one body psychological

tactile sensor and its uniqueness. This research can also allow researchers to broaden the concept of human tactile sensing and its applications.

1.3 Thesis Overview

This thesis is organized as in the following: Chapter 2 explains the human tactile sensing system and previous researches are introduced regarding the tactile sensors which can give ideas for the demonstration of the tactile sensor for detecting ‘pain’ sense. Structure and fabrication of the Zinc Oxide (ZnO) nanowire based tactile sensor and experimental set-up for measuring electrical output potential are presented in Chapter 3. The results generated when the ZnO nanowires experience the temperature and pressure variation and simple signal processing methods are presented in Chapter 4. Chapter 5 concludes the thesis with the implication of pressure and temperature sensor with the ZnO nanowire arrays in the field of tactile sensing technology.

II. **BACKGROUNDS**

2.1 Human Tactile Sensing System

Understanding human tactile sensing system will provide ideas for designing tactile sensors and the systems. This chapter describes the human tactile sensing mechanism and hints for demonstrating the tactile sensing system. Neurophysiology of human tactile system is explained in the following section.

The human sense of touch can be explained by the spatiotemporal perception of external stimuli through a large number of receptors distributed all over the body. They are categorized according to the functions, for example, mechanoreceptors-for pressure/vibration, thermoreceptors-for temperature, and nociceptors-for pain/damage [14]. Their number, per square centimeter area, is estimated to be 241 in the fingertips and 58 in the palm of adult humans [15]. The response to thermal stimulus is believed to be mediated by separate 'warm' and 'cold' thermoreceptor population in the skin. Interestingly, the nature of electrical discharge from various receptors in response to the external stimuli is found to be pyroelectric and piezoelectric [16].

Spatiotemporal limits and sensitivity to mechanical stimulus are important factors that the object recognition capability and directional sensitivity is decided. Spatial resolution indicates the smallest separation at which one can tell if he/she has been touched at two points. It varies across the human body: human fingertips have the highest value; face, toes, thigh and belly are followed [1]. One can resolve two points as close as 1 mm on the fingertips [17] however; the spatial resolution for the belly is 30 mm [18]. Skin microstructures like intermediate ridges enhance the tactile spatial acuity by transmitting magnified signals from surface of skin to the mechanoreceptors [19].

Regarding the temporal resolution, humans are capable of detecting vibration up to 700 Hz. In other words, human can detect a single temporal interval of about 1.4 ms [20]. The critical temporal separation for two events at different locations on fingertips is found to be on the order of 30-50 ms [21].

The pressure threshold and skin deformation are other common intensive measures of absolute tactile sensitivity. Normal mean threshold values are averaged about 0.158 g on the palm and about 0.055 g on the fingertips of men. The corresponding values for women are 0.032 g and 0.019 g, respectively [22].

The temperature sensitivity also varies with the body parts. For example, the temperature change of 0.16 ℃ and 0.12 ℃ from a temperature of 33 ℃ for warmth and cold, respectively, can be detected at human fingertips [23].

2.2 Hints for the Design of Tactile Sensing System

The design criteria of tactile sensing system can be formulated by previous discussions. Based on the findings reported in [1, 2], [24, 25], hints for the design of tactile sensing system is introduced.

1) It is desirable to have multi-functional sensors that can detect normal force, shear force, strain, tactile and thermal variables. The detection of parameters for high level interaction between the objects and the sensors including roughness and softness is also desired.
2) The spatial resolution of the tactile sensors should be about 1 mm for the fingertips.
3) Tactile sensors should detect both dynamic and static contact events. Appropriate transduction mechanism for tactile sensor is required.
4) The response time of the tactile sensor should be as fast as 1 ms.

5) High sensitivity of tactile sensor is required. Force sensitivity range is 15-90 wg and force sensitivity for the dynamic events is 0.01-10 N.
6) Wiring should be minimized for the simple fabrication and minimal cross-talk is desired.
7) Linearity and low hysteresis are desired.
8) Low power consumption and cost are also desired.

2.3 Previous Works

2.3.1 Robotic Tactile sensing system

The remarkable development of humanoid robots has led to emergence of interaction and learning issues as like human-beings [1]. Many researchers have studied the robotic tactile sensing system in order to design tactile sensors with fully integrated functions and the signal processing of tactile sensing signals. In robotics, tactile information is important that the robotic hands perceive the objects and take actions for the grasping and prevention of slip. Tactile sensors have been reported according to the transduction methods including resistive, capacitive, optical, ultrasonic, piezoelectric, magnetic, etc.

2.3.1.1 Resistive Sensors

Tactile sensors based on resistive mode of transduction have resistance values depending on the contact location and the applied force, in other words, piezoresistance. Resistive touch sensors are generally sensitive and economic but consume lots of power. Their other limitation is that they are not able to multi-touch. In [26], an improved design that allows measuring many contact points is presented. However, the limitation of contact force measurement still remains a critical problem. Piezoresistive touch sensors are made of mate-

rials whose resistance changes according to the force or pressure. Pang et al. demonstrate the interlocking-based strain-gauge sensor which can detect multiple mechanical loadings such as pressure, shear and torsion [27]. Using metal-coated, high-AR polyurethane-based nanofibers, three different loadings of pressure, shear and torsion is verified through the degree of interconnection and the electrical resistance of the sensor.

2.3.1.2 Capacitive Sensors

Capacitive sensor type has been widely used in robotics and displays. They can be made very small— which allows the construction of high spatial resolution sensor arrays. Furthermore, touch sensors based on capacitive mode of transduction are very sensitive, but parasitic capacitances and severe hysteresis are major drawbacks [2]. In [28], Lee et al. present capacitive type sensor which can measure normal and shear stress. Between the capacitor plates, a polydimethylsiloxane (PDMS) spacer layer with air gap is located. When an external force is applied, the air gaps are deformed that leads to a change in capacitance. Each sensor consists of four pairs of plates, and the pattern of changes in capacitance of the plates gives a measure of the magnitude and direction of the applied force. Kim et al. present another capacitive type tactile sensor which is highly sensitive, wearable, and multimodal carbon nano tube (CNT) based piezocapacitive sensory system [29]. It consists of a CNT microyarn circuitry incorporated with a stretchable Ecoflex dielectric onto PDMS substrates using a simple methodology. This sensor can detect a position under pressure of 0.4 Pa and exhibit fast response time of 63 ms. In particular, multimodal output electrical signals could be manipulated as a change of pressure, temperature, humidity variation and touch.

2.3.1.3 Optical Sensors

Tactile sensors with optical mode of transduction use the change in light intensity, at media of different refractive indices, to measure the pressure [1]. One of the issues of tactile sensors is wiring complexity as the number of sensors increases. Optical based sensors are immune to electromagnetic interference, flexible, sensitive, and fast but they are bulky. Loss of light by microbending and chirping, which cause distortion in the signal, are some other issues associated with optical sensors [2]. In [30], the force sensor based on polymer waveguides that is fast responsive, flexible and highly transparent is presented. The demonstration of simultaneous and multiple force detection was possible.

2.3.1.4 Ultrasonic based Sensors

The ultrasonic emission is generated when the motion of slip that contact point detection is possible from the acoustic ultrasonic. Ultrasonic based sensors have fast dynamic response and good force resolution [1, 2]. Shigeru Ando and Hiroyuki Shinoda present a 2 × 2 tactile sensing arrays using polyvinylidene fluoride (PVDF) [31]. The sensor consists of a flexible, hemispherical fingertip-like body and a quadruple PVDF sound-sensing matrix embedded at the center of the body which can withstand damage from rough touches. When the sensor is touched, the body transmits the longitudal waves inward.

2.3.1.5 Piezoelectric sensors

The piezoelectric materials generate charge in proportion to the applied force or pressure. Piezoelectric materials such as zinc oxide (ZnO), lead zirconate titanate (PZT), polyvinylidene fluoride (PVDF), etc., are desired for dynamic tactile sensing. Though quartz and ceramics have better piezoelectric properties however; the polymers such as PVDF are preferred in tactile sensors due to their excellent features [1]. PVDF-based sensors have high

flexibility, workability, and chemical stability. Also, sensors have high sensitivities and simple wiring is feasible. However, temperature sensitivity of piezoelectric materials is a major cause of concern [1, 2].

2.3.1.6 Magnetic sensors

Magnetism based sensors measure the change in flux density as a result of the applied force [1]. In [32], the flux is measured from the applied normal and lateral force by Hall-effect device. The sensors based on magnetic principle have a lot of advantages that include high sensitivity, good dynamic range, no measurable mechanical hysteresis, a linear response, and physical robustness. However, their usage is limited to nonmagnetic mediums [1].

2.3.2 Energy Harvesting Applications

Piezoelectric materials are good candidates for the energy harvesting applications. Recently, zinc oxide (ZnO), potassium niobate ($KNbO_3$), lead zirconate titanate (PZT), polyvinylidene fluoride (PVDF) based piezoelectric and pyroelectric nanogenerators have been reported and used to harvest mechanical energy or thermal energy. Nanogenerator based on the micro-patterned piezoelectric P(VDF-TrFE) polymer, polydimethylsiloxane (PDMS)-carbon nanotubes (CNTs) composite and graphene nanosheets is fabricated in [13]. The piezoelectric and pyroelectric outputs from strain and thermal gradients were obtained and showed the stretchability, mechanical durability and robustness of the device due to the micro-patterned design.

In 2006, the piezoelectric nanogenerators based on ZnO nanowire arrays are suggested for conversion of mechanical energy into electrical power [33]. The measurement

were performed by an atomic force microscopy (AFM) using a Silicon (Si) tip coated with Platinum (Pt) film. The ZnO has three key advantages that ZnO exhibits both semiconducting and piezoelectric properties, biocompatible and have various nanostructures. With ZnO nanowires, the self-powered device that does not depend on the battery can be realized. The first pyroelectric nanogenerators using ZnO nanowires for harvesting thermoelectric energy is demonstrated in [12]. The fabricated nanogenerator has a good stability, and the characteristic coefficient of heat flow conversion into electricity is estimated to be $\sim 0.05-0.08$ $\mathrm{Vm^2/W}$. This nanogenerator have potential of using pyroelectric nanowires to convert wasted energy into electricity for powering nano-devices.

From the two cases for the energy harvesting applications, the tactile sensor should be self-powered that does not depend on the battery. This implies that the tactile sensors on the robot hands, displays and other human-machine interfaces do not need power sources. Therefore, piezo-pyro electric materials can be good candidates for the tactile sensors.

2.4 Piezo-pyro Electric Nanowire

2.4.1 Principles of Piezoelectricity

Piezoelectricity is linear interaction between mechanical and electrical systems in non-centric crystals or similar structures. The direct piezoelectric effect is defined as the change of electric polarization proportional to the strain. If the application of an external mechanical stress gives rise to dielectric displacement, the material is said to be piezoelectric. It should be noted that the piezoelectric effect strongly depends on the symmetry of the crystal. A crystal having sufficiently low symmetry produces electric polarization under the influence of external mechanical force. The converse piezoelectric effect is the opposite

operation of direct piezoelectric effect; whereby a piezoelectric crystal becomes strained if an external electric field is applied.

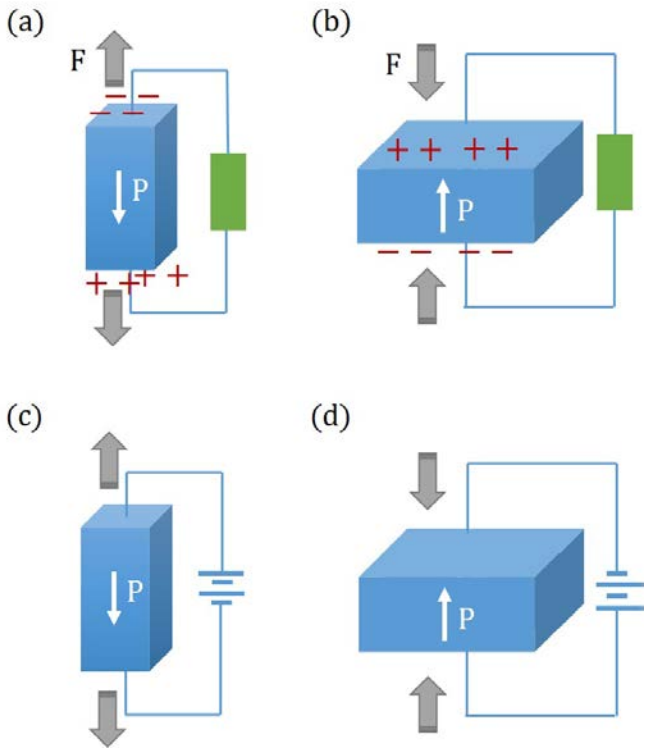

Fig. 2.1 Principles of the direct and converse piezoelectric effects. Direct piezoelectric effects; (a) When the strain is applied to the material, the polarization charges covered the surface of the material, (b) When a compressional force is induced, the polarization is the opposite from that of (a), Converse piezoelectric effects; When the positive (c) and negative (d) electric field is applied to the material, the material is deformed.

In Fig. 2.1, the schematic of piezoelectric effect is represented. If a compressional force F is induced, the polarization P, parallel to the thickness is proportional to the stress T=F/A. Hence, the piezoelectric polarization charges on electrodes covering the major faces A is proportional to the force causing the strain. If we apply tension, the sign of pressure is reversed and the sign of the electric polarization reverses as well. When an electric field E is applied along the thickness of the plate the quartz plate is deformed [34].

2.4.2 Principles of Pyroelectricity

The spontaneous polarization change due to the mechanical stress is called piezoelectric effect as mentioned earlier. The spontaneous polarization is also temperature dependent and it is called pyroelectric effect. The converse effect, the change of the temperature generated by the external electric field, is called electrocaloric effect. Every pyroelectric material is also piezoelectric material. The pyroelectric coefficient is described as the

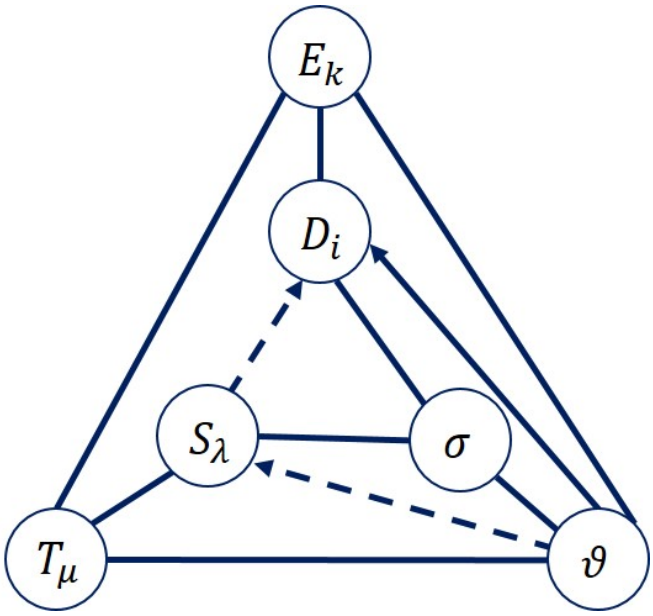

Fig. 2.2 Primary and secondary pyroelectric effects.

change in the spontaneous polarization vector with temperature. Let us choose the independent variables; temeprature ϑ, electric field E_k and mechanical stress T_μ.

$$D_i = p_i^T \Delta\vartheta \quad (1)$$

Eg. 1 is derived from $p_i^T = \frac{\partial D_i}{\partial \vartheta}$ [34]. This effect is schematically illustrated in Fig 2.2 by the full arrow $\vartheta \rightarrow D_i$. Similar relationship between electric displacement D_i and the temperature change $\Delta\vartheta$ could be derived through the dashed arrows $\theta \rightarrow S_\mu$ and $S_\mu \rightarrow D_i$. The temperature change results in mechanical strain S_μ due to the thermal expansion. Mechanical strain

is further related to the electric displacement D_i due to piezoelectric effect. For the independent variables $\Delta\vartheta$ and S_μ at constant electric field E_k, we can get the electric displacement [34].

$$D_i = p_i^s \Delta\vartheta + e_{i\lambda}^{\vartheta} S_\lambda \quad (2)$$

Similarly, the mechanical strain at constant electric field is

$$S_\lambda = \alpha_\lambda^E \Delta\vartheta + s_{\lambda\mu}^{\vartheta,E} T_\mu \quad (3)$$

Combination of Eqs. (2) and (3) tend to the equation

$$D_i = (p_i^s + \alpha_\lambda^E e_{i\lambda}^{\vartheta})\Delta\vartheta + e_{i\lambda}^{\vartheta} s_{\lambda\mu}^{\vartheta,E} T_\mu \quad (4)$$

If the mechanical stress is held constant, Eq. (4) reduces to

$$D_i = (p_i^s + \alpha_\lambda^E e_{i\lambda}^{\vartheta})\Delta\vartheta$$

Electric displacement D_i in both eqs. (1) and (4) is expressed as a function of the temperature change at the same conditions. It results in the following relationship between pyroelectric coefficients.

$$p_i^T = p_i^s + \alpha_\lambda^E e_{i\lambda}^{\vartheta}. \quad (5) \text{ [34]}$$

Therefore the pyroelectric coefficient at constant mechanical stress is equal to the sum of two terms. First term in eq. (5) represents the pyroelectric coefficient at constant strain so called primary pyroelectric effect. Pyroelectric coefficients describes the electric displacement as a function of the temperature change for the sampled with compensated thermal expansion. Microscopic origin of this phenomenon is from the crystal deformation. Such effect might reach especially high values at the phase transitions not related with piezoelectricity. However, the primary pyroelectric effect at the room temperature is normally small in linear pyroelectric materials. Primary effect amounts just 2-5% of the total pyroelectric effect. Second term in eq. (5) represents the piezoelectric effect contribution to the total pyroelectric effect. It is illustrated by the dashed arrows in Fig. 2.2 $\vartheta \rightarrow S_\lambda \rightarrow D_i$. This effect is called secondary

pyroelectric effect. Spontaneous polarization shows changes due to this effect even if no structural changes in crystal take place. Temperature changes in lattice constant are connected with the changes of elementary dipole moments and therefore result in the polarization [34].

2.4.3 Zinc Oxide (ZnO) Nanowire

For pressure and temperature sensor arrays, various transduction mechanism can be applied to detect pressure and temperature output levels. The most common principles such as resistive and capacitive type sensors, are widely adopted in smart phones and various displays [35]. However, the resistive type has limitation for multi-touch applications and capacitive type has low sensitivity to be utilized in highly sensitive pressure and temperature sensing applications [36]. The ZnO has gained substantial interest in the research

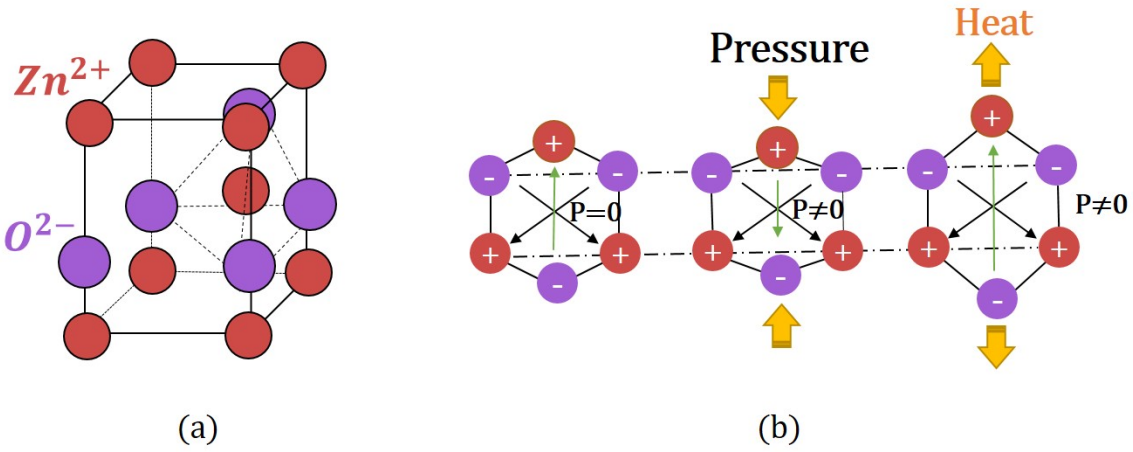

Fig. 2.3 The structure of the ZnO and the principles of polarization under pressure and temperature variation. (a) Wurtzite structure model of ZnO, which has piezo-pryo electric effects. (b) When the ZnO is under compressive pressure, the net dipole moment is generated. When the heat is induced to the crystal, a similar distortion occurred in the opposite way.

community because of its several advantages such as high sensitivity, high resolution, being self-powered and multi-touch capability. Also, the ZnO based device can be fabricated

below 100 ℃ which indicates that the fabrication on the flexible substrate is possible. If we utilize the ZnO nanowire as tactile sensor, we can get relatively high piezoelectric coefficient due to the structural confinement of the nanowires in the radial direction unlike the low piezoelectric coefficient of bulk ZnO [37]. In Fig. 2.3, the principle of piezo-pyro electric effect is described to understand the mechanism of pressure and temperature sensing. Under conventional conditions, the ZnO has the wurtzite structure, which has a hexagonal unit cell space group C6mc and lattice parameters a=0.3296, and c=0.52065 nm. The oxygen anions and Zn cations form a tetrahedral unit. The entire structure of ZnO can be described as a number of alternating planes composed of tetrahedrally coordinated oxygen anions and Zn cations which lacks of central symmetry [38]. Piezo-pyro electric effect is due to the atomic scale polarization. As shown in Fig. 2.3 (a), oxygen anion is surrounded by the Zn cations tetrahedrally. The center of gravity of the negative charges is at the center of the tetrahedron. By exerting a pressure on the crystal, the tetrahedron will experience a distortion and the center of gravity of the negative charges will no longer coincide with the position of Zn cation at the center. Therefore the net dipole moment is generated. If all of the tetrahedral in the crystal have the same orientation or some other mutual orientation that does not allow for a cancellation among the dipoles, the crystal will have a macroscopic dipole. When the heat is induced to the crystal, a similar distortion occurred in the opposite way. The primary pyroelectric effect at the room temperature is small that it amounts just 2-5 % of the total pyroelectric effect [34]. Thus, the piezoelectric effect contribution to the total pyroelectric effect will be dominated with the opposite electric dipole moments.

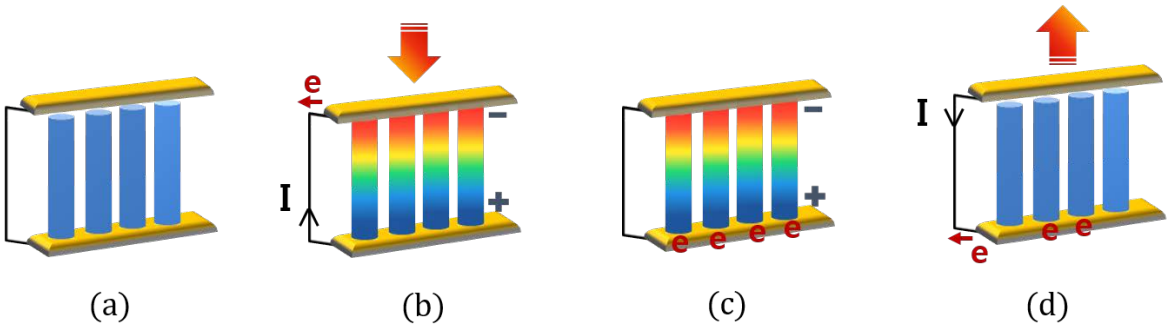

Fig 2.4 The mechanism of pressure sensing using ZnO nanowires. (a) The ZnO nanowires and Au electrode is integrated for the sensor. (b) When the compressive force is applied to the sensor, the ZnO nanowire generate piezoelectric potential and the electrons flow from the top electrode to the bottom electrode through the external circuit. (c) The potential maintained due to the schottky barriers between ZnO nanowires and the electrodes under the pressure. (d) The piezoelectric potential dissipated when the pressure is removed. The electrons flow back via the external circuit.

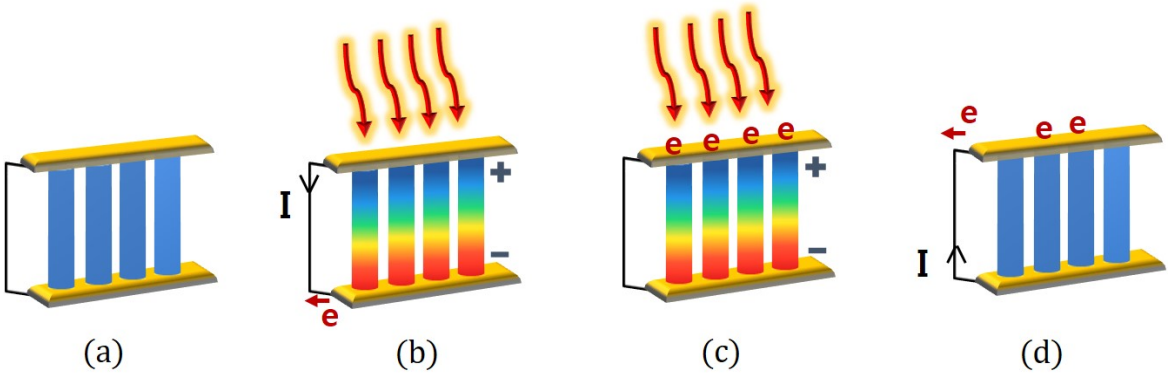

Fig 2.5 The mechanism of temperature sensing using ZnO nanowires. (a) The ZnO nanowires and Au electrode is integrated for the sensor. (b) When the temperature of sensor increased, the ZnO nanowire generate pyroelectric potential and the electrons flow from the bottom electrode to the top electrode through the external circuit. (c) The potential maintained due to the schottky barriers between ZnO nanowires and the electrodes under the temperature variation. (d) The pyrooelectric potential dissipated when the temperature source is removed. The electrons flow back via the external circuit.

By utilizing intrinsic properties of ZnO nanowire with the bottom and top capac-

itive electrodes, pressure and temperature sensing is described as shown in Fig. 2.4 and 2.5. The bottom and top electrodes and the ZnO nanowires create Schottky barriers which act as capacitive electrodes. When pressure is applied to the ZnO nanowires, the ZnO nanowires are under uniaxial compression and electrons will flow from the top to the bottom through external circuit. In the meantime, the negative peak is detected and the electrons are accumulated around the bottom electrodes due to the Schottky barrier blocking the electron flow through the ZnO nanowires until removing external pressure. When the pressure is released from the ZnO nanowires, the electrons flow back via the external circuit, generating a positive electric pulse. In case of heat transfer to the ZnO nanowires, the ZnO nanowires expand and generate the opposite dipole moment of compression from external pressure. Therefore, the positive electric pulse is generated when the heat is induced, the electrons flow from the bottom to the top electrode. The electrons are blocked by the Schottky barrier between the gold (Au) and ZnO nanowires. When the heat source is removed from the ZnO nanowires, the accumulated electrons flow back creating a negative electric pulse. The piezo-pyro electric potential is linearly proportional to the magnitude of the ZnO nanowire. Therefore, if the pressing force or temperature is increased on the nanowires, their deformation becomes larger, and the electric output will linearly scale up [38].

2.4.4 Thermoelectric Effects

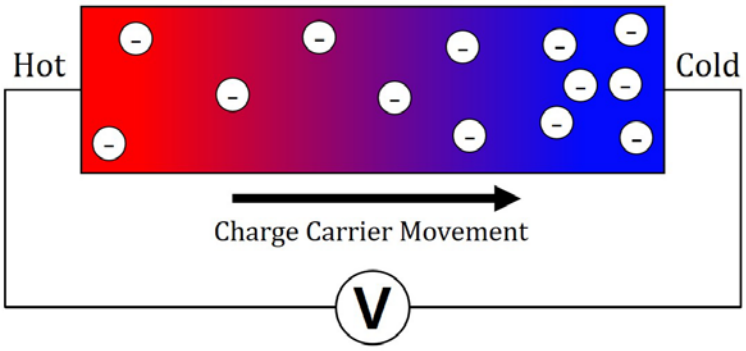

Fig. 2.6 The principle of thermoelectric effects.

Thermoelectric effects involve a fundamental interplay between the electronic and thermal properties of a system. These effects are most often observed by measuring electrical voltage and current induced by thermal gradients. The two primary thermoelectric effects are the Seebeck effect and the Peltier effect. When a conductive material is subjected to a thermal gradient, ΔT charge carriers migrate along the gradient from hot to cold; this is the Seebeck effect. In the open-circuit condition, charge carriers will accumulate in the cold region, resulting in the formation of an electric potential difference, ΔV as shown in Fig. 2.6. The potential difference developed per unit temperature difference, or $S = \frac{dV}{dT}$ is introduced.

The Seebeck effect describes how a temperature difference creates charge flow, while the Peltier effect describes how an electrical current can create a heat flow. Therefore, the Seebeck effect and the Peltier effect are then opposite of one another [39].

III. **EXPERIMENTAL DETAILS**

3.1 Structure and Fabrication of Tactile Sensor

The concept of tactile sensor is derived from human tactile sensing mechanism. As shown in the Fig. 3.1, the skin of a human finger deforms differently regarding to the objet characteristics. When the sharp object such as needle and pencil lead pricked human skin, the deformation occurs in a very small area of the skin, however a blunt object including eraser and earplug deforms a larger area of the skin. According to the inputs received, receptors beneath the human skin arouse several feelings such as pain, roughness and softness. Focusing on the tendency of deformation in human skin, simple electro-mechanical structure design can mimic the human tactile sensing [36]. By distributing a number of active sensors, a sensor array device can detect different pressure and temperature levels, which can deliver ‘pain’ warning signal.

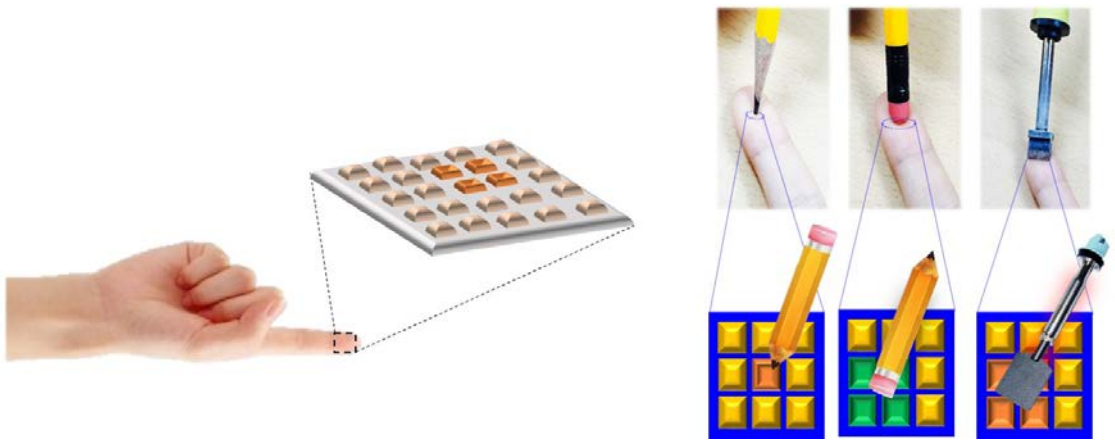

Fig. 3.1 Schematic of tactile sensor arrays. The pressure levels and the distribution shape of tactile sensors can induce ‘pain’ or ‘smooth’ feeling signals. There is a hot ‘pain’ warning signal when the high temperature input is induced to the tactile sensor arrays.

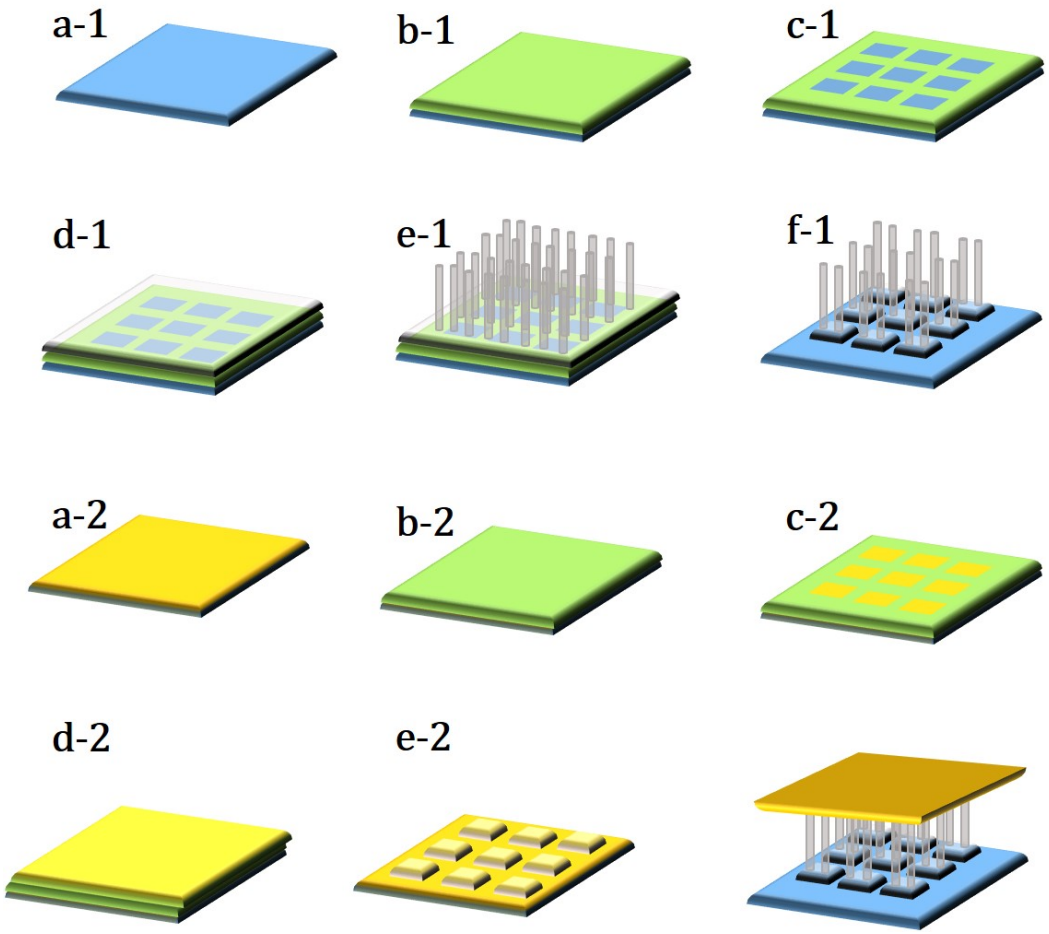

Fig. 3.2 The fabrication process of the ZnO nanowire based tactile sensor. The fabrication process of bottom electrode and ZnO nanowire growth: a-1) Cleaning of Si substrate. b-1) Spin coating of photoresist. c-1) Photolithography. d-1) ZnO Seed layer deposition. e-1) ZnO nanowire growth. f-1) Lift-off. The fabrication process of top electrode: a-2) Polyimide film cleaning. b-2) Spin coating of photoresist. c-2) Photolithography. d-2) Cr/Au layer deposition. e-2) Lift-off. The complete tactile sensor is demonstrated on the right corner.

The detailed fabrication process of the ZnO nanowire based tactile sensor is following. By using photolithography system, the 3 × 3 array is patterned on the Silicon (Si) substrate. Before coating the photoresist (PR) (AZ GXR-601), which is positive type, hexamethldisiloxane (HMDS) was treated to enhance the adhesion between the PR and the substrate. PR was spin-coated on a Si substrate with 3000 revolution per minute (rpm). After coating the PR, the coated substrate was baked on a hot plate in 100 ℃ for 2 minutes for

hardening the PR. The PR was exposed by ultraviolet ray (UV) with 51.8 mJ/Cm^2 through the 3 × 3 spuare arrays pattern in photo-mask. Then the polymer chains of PR is loosely bounded by UV exposure. Then, the sample is developed by dipping in AZ-developer for 1 minute and 30 seconds. After developing, the samples were rinsed by deionized (DI) water and blown by argon (Ar) gas. The 100 nm thick of gold (Au) layer and 100 nm thick chrome (Cr) layer were deposited by using a radio frequency (RF) magnetron sputtering system at an input power of 200 W and pressure of 5 mTorr. The Cr layer was sputtered to enhance the adhesion between the Si substrate and the Au layer. Next, the 3 × 3 bottom electrode of Au was obtained through the lift-off process dipping in acetone and isopropyl alcohol (IPA) by ultrasonication. The photolithography process is performed again to grow the ZnO nanowires on the bottom electrode. The 3 × 3 square patterned array without interconnects is made right on the bottom electrode by alignment process. The ZnO seed layer is sputtered on the whole sample. After that, we grow the ZnO nanowires by hydrothermal method which is simple, ensure low temperature process. The nutrient solutions with zinc nitrate hexahydrate and hexamethylenetetramine (HMTA) were prepared. Each of solution was composed of a 25 mMol/900 mL. 300 mL of two solutions were mixed in the bottle and the sample which was fixed in a Teflon holder was put in the bottle. Then, the bottle was put inside a 90 ℃ oven for total 48 hours. Every 12 hours, the nutrient solution should be refreshed with the new one. After the ZnO nanowire growth, the sample was put in the acetone and IPA for lift-off process. Then the ZnO nanowires remained only on the bottom Au layer. For the top electrode fabrication, the polyimide film is cleaned. Same procedure for the 3 × 3 pattern is made as explained above. Then the Cr/Au deposition is performed by the RF sputtering system. Then the lift-off process is done for the Au top electrode. Then the ZnO nanowire sample and the top electrode is aligned for the integrated tactile sensor. The schematic of fabrication process is shown in Fig. 3.2. The fabricated 3 × 3 arrays are shown in Fig. 3.3.

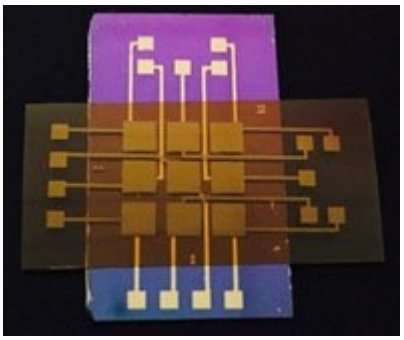

Fig. 3.3 The fabricated 3 × 3 array type ZnO nanowire based tactile sensor.

3.2 Experimental Setup

To measure the electrical signals of tactile sensor, digital phosphor oscilloscope (Tektronix DPO3034) was used. The voltage signals are directly measured by oscilloscope but the current signals were measured by a low noise current preamplifier SR570. This enables measurement of clearer electrical signals. Also, the broad range of electric current signal could be measured. In order to inducing the pressure on the sample, a piezoelectric measurement system was made. The system consisted with an X, Y and Z linear position stage, motion actuator, a load cell and a system control.

IV. **RESULTS AND DISCUSSIONS**

4.1 ZnO Nanowire Characteristics

There are two conditions in the ZnO nanowire growth that one nutrient solution material is a zinc nitrate hexahydrate and the other is a zinc chloride ($ZnCl_2$). In order to compare and find the optimal condition for the ZnO nanowire growth, the characteristics of each nanowires have been studied. Fig. 4.1 shows the scanning electron microscope (SEM) images of the ZnO nanowire grown by the $ZnCl_2$ nutrient solution. The average length and diameter of nanowires is 8 um and 100 nm respectively. Fig. 4.2 shows the SEM images of the ZnO nanowire grown by the zinc nitrate hexahydrate nutrient solution. The average length and diameter of nanowires is 6 um and 80 nm respectively.

The photoluminescence (PL) spectrum of the ZnO nanowires usually exhibits

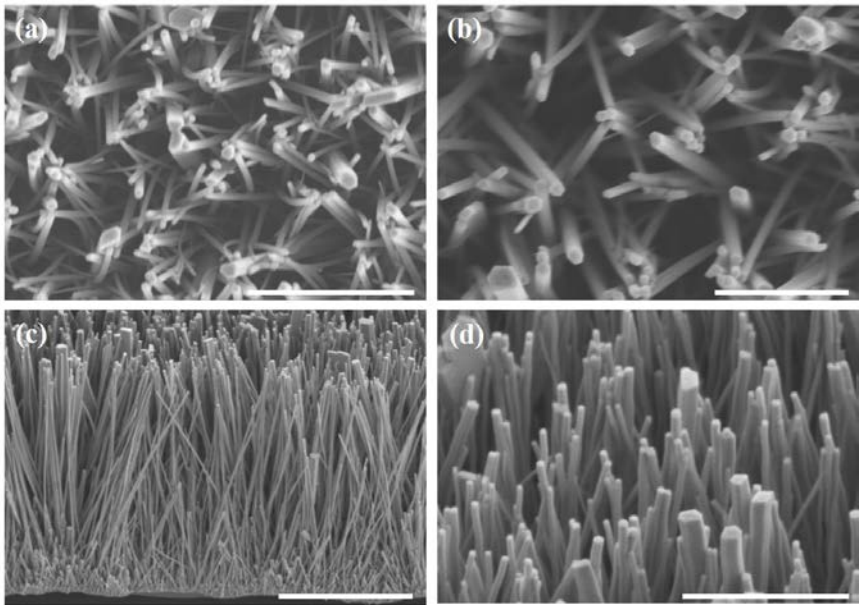

Fig. 4.1 The SEM images of the ZnO ($ZnCl_2$) nanowires on Au bottom electrode. (a, b) Top view of the ZnO nanowires. (c, d) 45° tilted view of the ZnO nanowires. (The scale bar is correspond to 2um (a, d), 1um (b), 5um (c).)

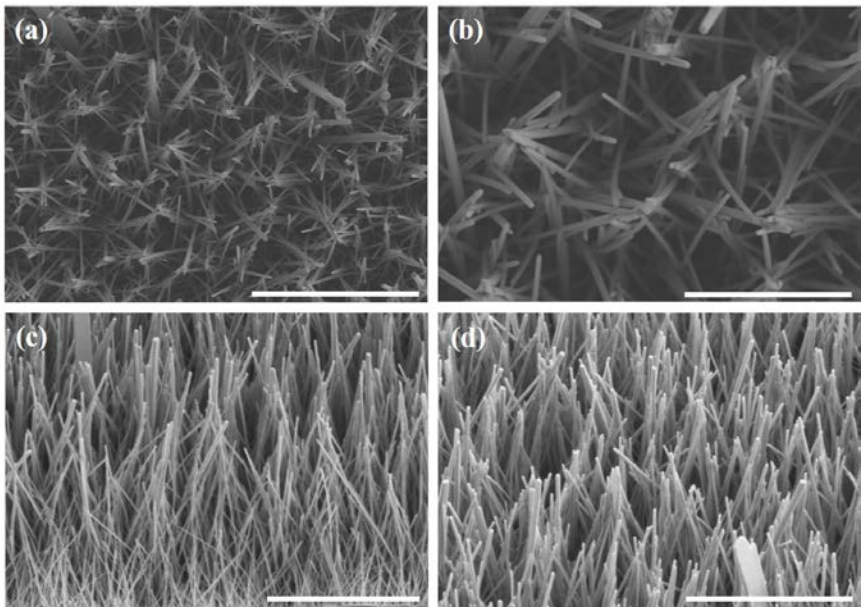

Fig. 4.2 The SEM images of the ZnO (zinc nitrate hexahydrate) nanowires on Au bottom electrode. (a, c) Top view of ZnO nanowires. (c, d) 45° tilted view of ZnO nanowires. (The scale bar is correspond to 5um (a, c, d), 2um (b).)

two strong-luminescence bands, a band edge emission (UV band) and a visible broad band. The UV band is attributed to the direct recombination of excitons through an excition-exciton collision process. However, the visible broad band originated from a variety of deep level defects such as vacancies and both oxygen and zinc interstitials. Fig. 4.3 is PL data of as-grown ZnO nanowires of two nutrient solution cases. The red line shows the results of the $ZnCl_2$ and the blue line corresponds to the zinc nitrate hexahydrate solution. The UV

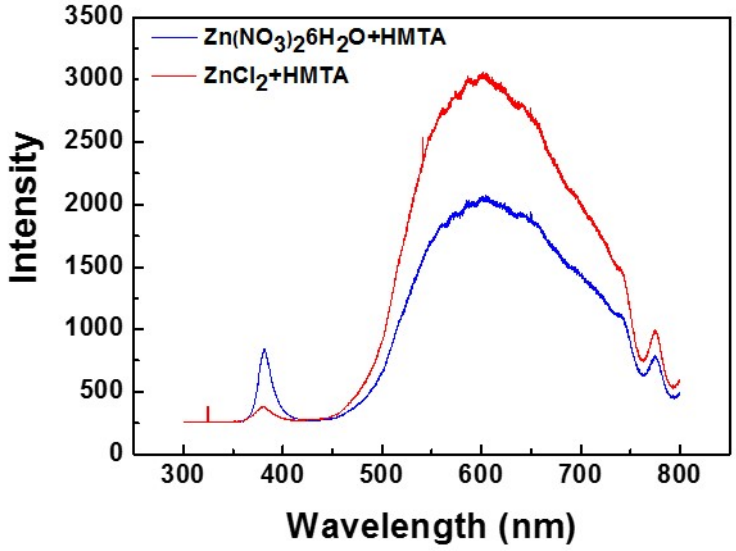

Fig. 4.3 The Photoluminescence (PL) spectrum of the ZnO nanowires. The nutrient solution difference of zinc ions is observed by aspect ratio between a band edge emission (380nm) and a visible broad band. The ZnO nanowires grown by the $ZnCl_2$ nutrient solution have more defects than the ZnO nanowires grown by zinc nitrate hexahydrate nutrient solution.

emission intensity of nanowires grown by the zinc nitrate hexahydrate is stronger than nanowires grown by the $ZnCl_2$. In addition, the defect emission of nanowires grown by the $ZnCl_2$ is intenser than the nanowires grown by the zinc nitrate hexahydrate. This results implies that there are more free carriers in the ZnO nanowires when the nanowire is grown by the $ZnCl_2$ nutrient solution. If we make use of the free carriers in the ZnO nanowires for the temperature detection, the appropriate condition for the growth of the ZnO nanowire is

the $ZnCl_2$. Fig. 4.4 shows the current signals when the heat is induced to the Au top electrode and the Au bottom electrode. There is a big difference between two cases; When the ZnO

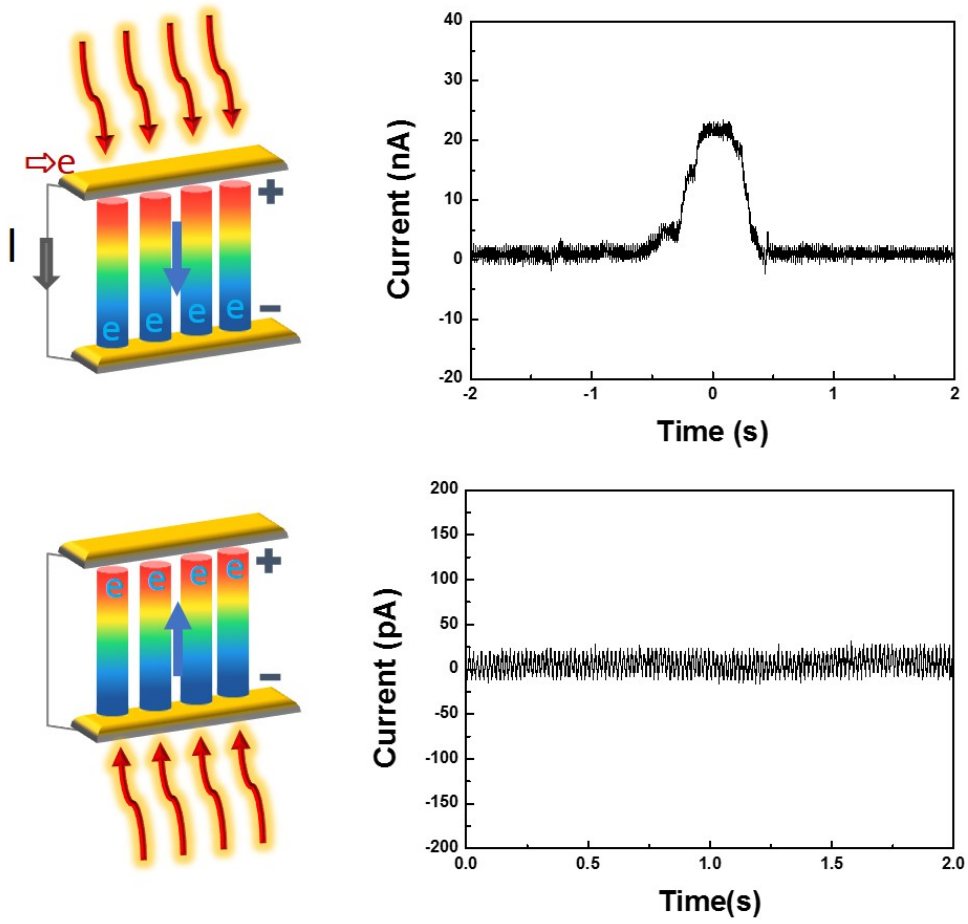

Fig. 4.4 The pyroelectric current signals and the Seebeck effect of free carriers in the ZnO nanowires. The current signal is about 20 nA when the heat is induced to the Au top electrode and the current signal is not detected when the heat is induced to the Au bottom electrode.

nanowire undergoes the temperature variation, the polarization in the ZnO is generated as shown in the Fig. 4.4. Furthermore, the free carriers inside the ZnO nanowires respond to the heat source that free carriers goes the opposite way from the point temperature increasing.

When the temperature increases on the top electrode of the sensor, the free carriers goes down toward the bottom electrode. As a result, the polarization generated in the ZnO nanowires does not affected by free carriers' movements. The positive current is observed due to polarization in the ZnO nanowires with the movement of free carriers. However, when the

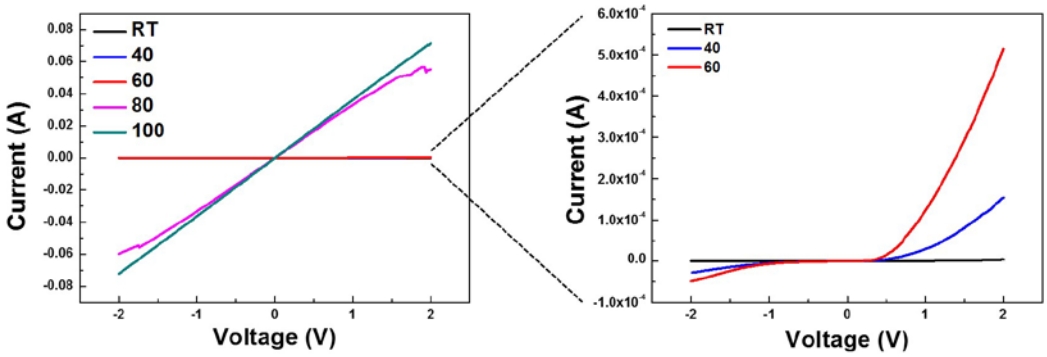

Fig. 4.5 The current-voltage characteristics between the Au bottom electrode and ZnO nanowire. The room temperature, 40 ℃ and 60 ℃ data are enlarged on the right side.

heat is induced from the bottom electrode, the free carriers goes upside in the ZnO nanowires and they weakens the polarization inside of the ZnO nanowires. As shown in the Fig. 4.4, the current flows almost zero. This implies that we can use this phenomenon as temperature and

pressure sensor by utilizing characteristics of the pyroelectric effect and the Seebeck effect of defects inside of the ZnO nanowires. The positive peak is observed when the pressure is induced and the negative peak is followed when the pressure released. That derives from the polarization inside of the ZnO nanowire as described before. When the heat is induced to the ZnO nanowire, adverse peak should be generated because the polarization is the opposite from the piezoelectric effect. In other words, when the temperature increases from the heating source the positive peak is generated and the negative peak should be followed as the temperature decreases. However, as shown in Fig. 4.4, only positive peak is observed when the temperature increases. The reason for this phenomenon is explained by the collapse of Schottky barrier in high temperature and the gradient of temperature decreasing. In Fig. 4.5, the current-voltage curve between the Au bottom electrode and ZnO nanowire from the room

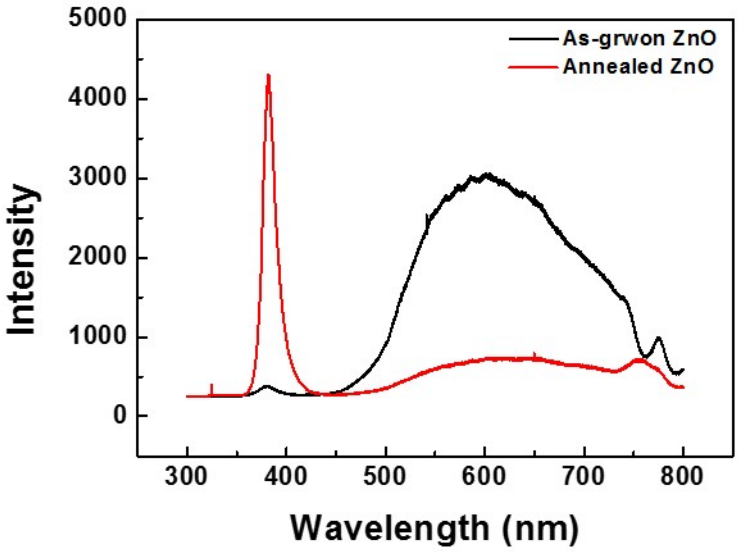

Fig. 4.6 The PL data for the as-grown ZnO nanowires and annealed ZnO nanowires. The defect level is highly decreased compared with the as-grown ZnO nanowires.

temperature to 100℃. The Schottky barrier between the Au and ZnO restrained the electron flow that the current-voltage curve shows asymmetric characteristics. This enables the peak generation due to polarization change inside of the ZnO nanowires. However, as temperature

increases above 80℃, current-voltage curve shows Ohmic characteristic that the current increases linearly as the voltage increases. Let us consider when the situation when the burning-hot object such as soldering iron heat the ZnO nanowire based tactile sensor. The moment that soldering iron makes temperature increasing, the positive peak is observed at first. If the temperature goes up consistently above the temperature of 80 ℃, which makes the Schottky barrier collapse, the charges accumulated on the Au top electrode disappeared. As a result, the negative peak, as expected to observe when the soldering iron does not affect the ZnO nanowires anymore, is not generated. Another reason could be the temperature gradient difference between increasing and decreasing. As temperature increases as the hot object touched the tactile sensor, the gradient of temperature increasing is a lot higher than the temperature gradient of decreasing when the heat source is removed. The pyroelectric current coefficient can be described as where I is the pyroelectric current, A is the electrode area, dT/dt is the rate of change in temperature. The temperature change when the soldering iron heat the ZnO nanowire is high enough to generate pyroelectric current, but the change in temperature decreasing is a lot lower than that of increasing because the ZnO nanowires are not in the heat rejecting environment.

Fig. 4.6 shows the PL data of the as-grown ZnO nanowires and annealed ZnO nanowires. Annealing of the ZnO nanowires is proceeded with chemical vapor deposition (CVD) system. At first, the 100 sccm Ar gas is flowed in the CVD vacuum chamber. Then the CVD chamber temperature is set to be 350 ℃. In order to compare the electrical properties, the as-grown ZnO nanowire sample and annealed sample were measured when there are pressure and pressure with temperature inputs. Fig. 4.7 shows the piezo-pyro electrical output

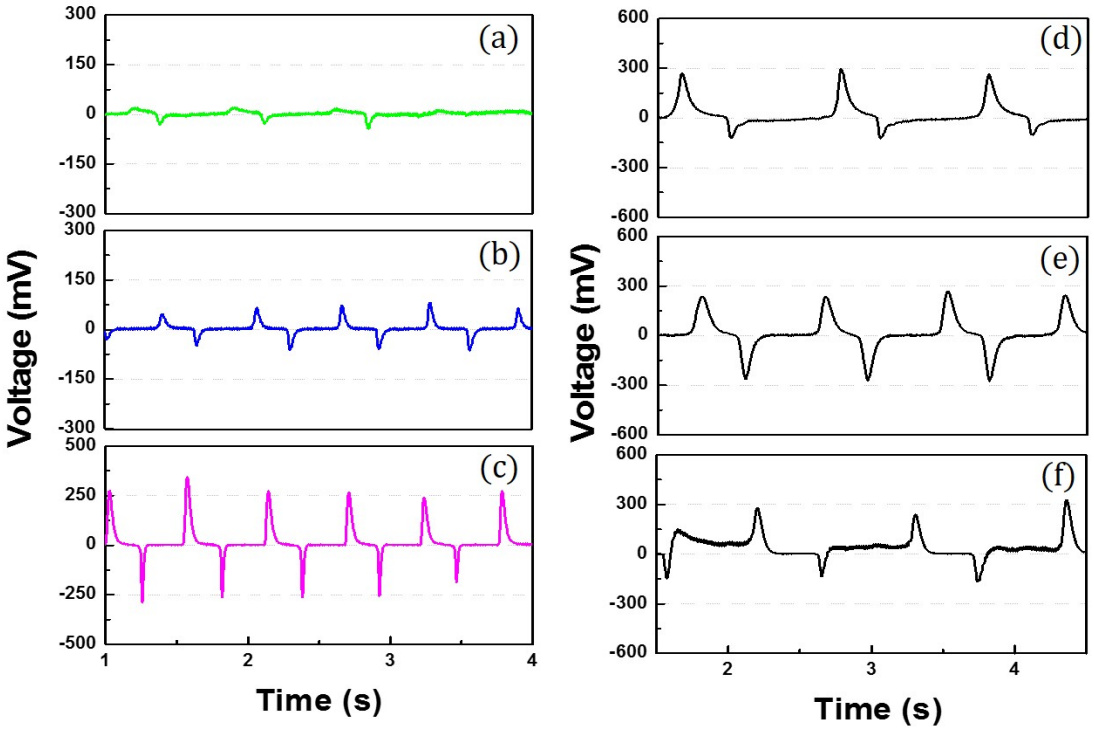

Fig. 4.7 The piezo-pyro electrical output voltages of annealed ZnO nanowires. (a) The electrical voltages when the ice is pressed on the tactile sensor. (b) The electrical output voltages when the sample is under pressure by human finger. (c) The electrical output voltages when the sample is pressed with the object heated from hot plate. The piezo-pyro electrical output voltages from the as-grown ZnO nanowires. (d) The electrical output voltages when the ice is pressed on the tactile sensor. (e) The electrical output voltages when the sample is under pressure by human finger. (f) The electrical output voltages when the sample is pressed with the object heated from hot plate.

voltages from each of samples. Fig 4.7 (a-c) is the electrical output of annealed sample. Electrical output in Fig. 4.7 (a) is when the ice is pressed on the tactile sensor. Fig. 4.7 (b) shows piezoelectric output voltages when the sample is under pressure by human finger. Fig. 4.7 (c) is when the sample is pressed with the object heated from hot plate. When the tactile sensor was under temperature variation from original state, the pyroelectric signal expected to be detected as dc level shift between the serial negative and positive piezoelectric output peaks. However, from the annealed sample, this electrical phenomena is not observed. In contrast to annealed sample, the as-grown ZnO tactile sensor shows the pyroelectric signal when the sample is under low temperature (Fig. 4.7 (d)) and high temperature (Fig. 4.7 (f)) with pressure.

4.2 Pressure and Temperature Sensing

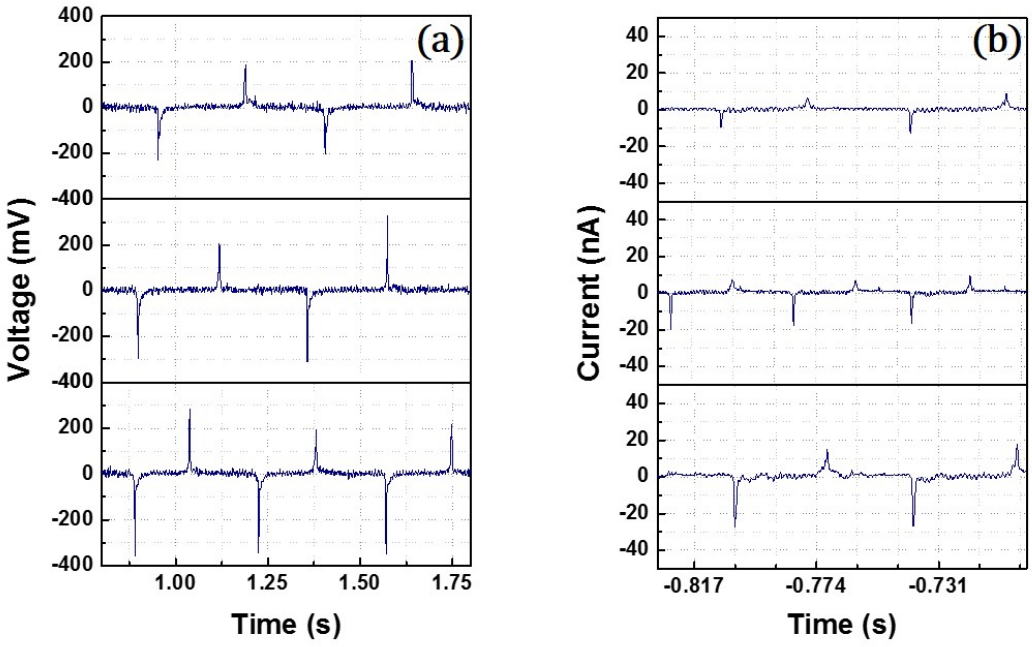

Fig. 4.8 The piezoelectric output voltages and currents when the tactile sensor is under pressure. The voltage output and current output level increased as the input pressure increasing.

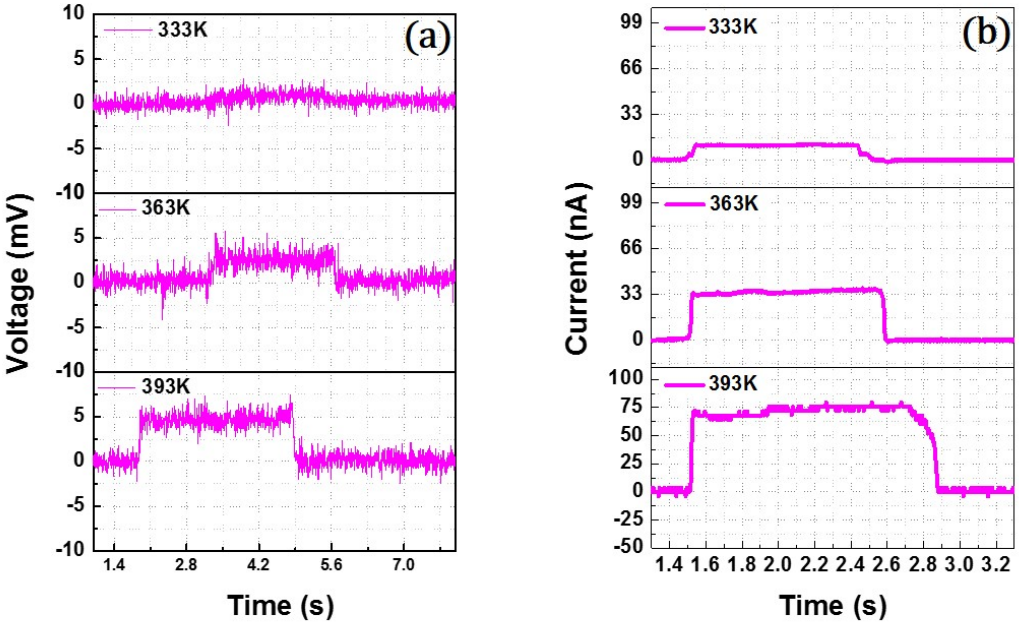

Fig. 4.9 The pyroelectric output voltages and currents when the tactile sensor is under temperature variation. The voltage output and current output level increased as the input pressure increasing. The sensitivity of voltage output according to the temperature is lower than that of currents. The pyroelectric current output is suitable for detection of temperature inputs.

The open-circuit voltages and short-circuit currents of the tactile sensor were measured by inducing increasing pressure or heat with a soldering iron. When the pressure was induced to the sensor by the pressure measurement system, the voltage and current signals were generated as shown in Fig. 4.8. A negative peak was observed when the sensor was in the pressed state and the positive peak was generated when the sensor was released. According to the magnitude of input pressure induced to the sensor, the piezoelectric signal is generated that those results can be analyzed whether the input pressure is high or not. High pressure can be categorized as painful sense, and detection of this signal is meaningful for the tactile sensor. Another pain sense can be the burning-hot temperature that can cause severe damage to the humanoid interface. Fig. 4.9 shows the voltage and current output signals re-

sponse to the temperature gradient generated by the soldering iron. The voltage level of signal started to increase, for example, the sample was heated by soldering iron from 60 ℃ to 120 ℃. The level shift of voltage signal depends on the temperature of soldering iron. When the temperature of the soldering iron increased, the output voltage signals increased as well. The voltage signals ranged from 2 mV to 7.6 mV. From the pyroelectric effect of the ZnO nanowire that the electrical signals are generated due to the external heat stimuli, sensors can detect the urgent situation which may harm the humanoid interfaces, robotics, wearable devices and prosthetic arms.

4.3 Analysis of Various Tactile Stimulus Scenarios

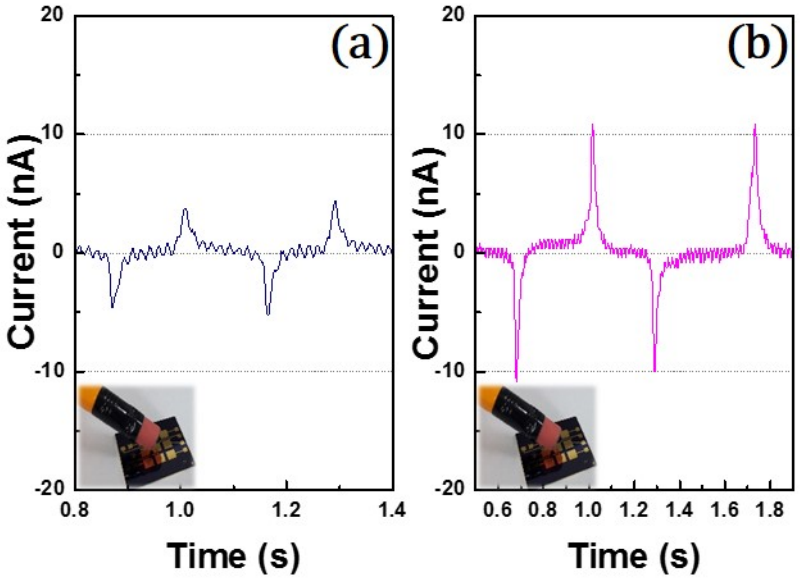

Fig. 4.10 The piezoelectric current output from one cell when the object touched the sensors with high pressure (a) and low pressure (b).

Fig. 4.10-12 shows several combinations of signals of pressure and temperature inputs. Fig. 4.10 is when the low pressure and low temperature inputs were induced that does

not generate ‘pain’ feeling such as finger touch. When the pencil eraser contacted to the sensor, the negative peak is observed and the positive peak is followed when the pencil is released from the sensor. If the threshold current level is set above the 5 nA level, the signal in Fig. 4.10 (b) does not generate ‘pain’ warning signal. Fig. 4.11 (a) is when the human finger

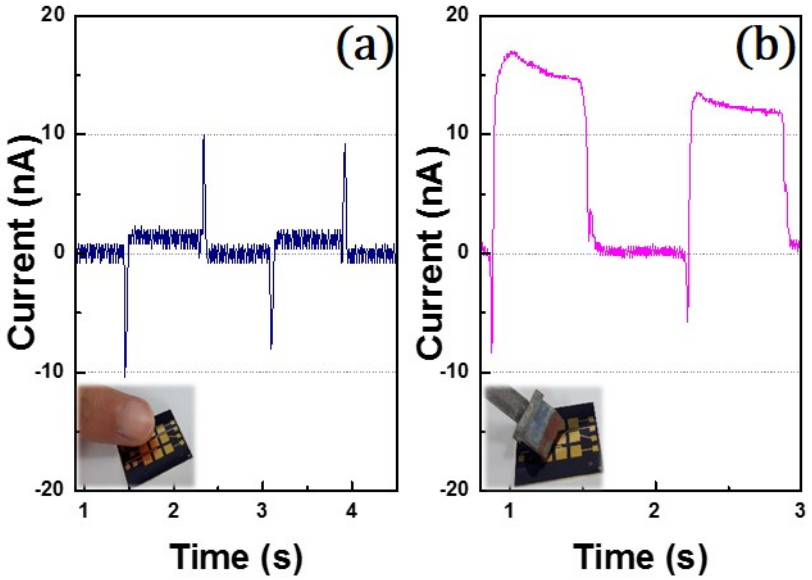

Fig. 4.11 The piezo-pyro electric current outputs from one cell when the human finger (a) and the soldering iron (b) touched the sensors.

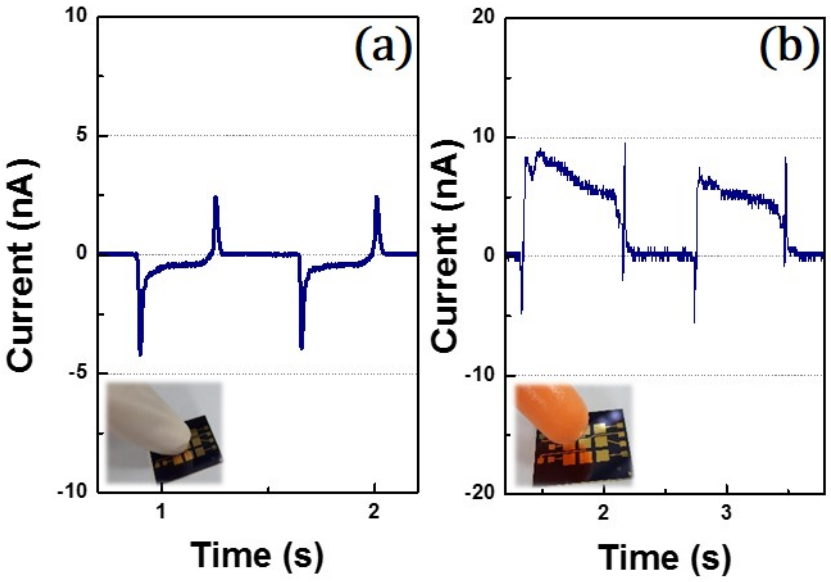

Fig. 4.12 The piezo-pyro electric current output from one cell when the ice (a) and the heated puff (b) touched the sensors.

touched the sensor. We can find negative peak at the point when the finger pricked the sensor. Unlike Fig. 4.10, between two of peaks, there is broad upside current flow is observed in response to the temperature increasing from human body temperature. Fig. 4.11 (b) is when the burning hot input is induced to the sensor from soldering iron. Fig. 4.12 is the case when the cool object such as ice touched the sensor. There are normal piezoelectric current as like Fig. 4.10. The only difference is that the current level shift between two peaks is negative. Fig. 4.12 (b) is the current output signals when the heated puff touched the sensor. The negative and positive pulses are observed as the puff touched and released. Also, the heat from the puff generated the dc level shift as like Fig. 4.11. These results show that the ZnO nanowire-based tactile sensor could have various input scenarios: 1) Low (High) pressure; 2) Low (High) temperature; 3) Low (High) pressure with Low (High) temperature. From the random electrical signals, we can easily be separated and sorted into ‘pain’ and ‘no-pain’ signals.

4.4 Signal Processing

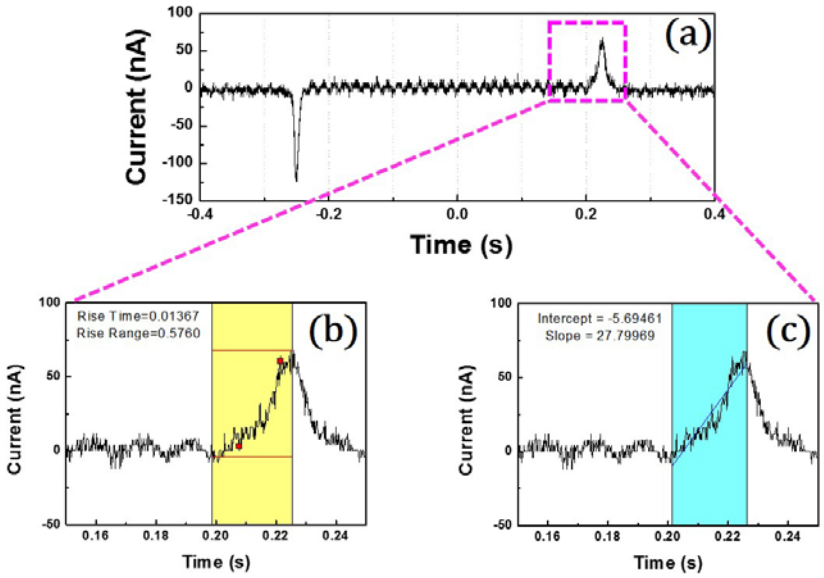

Fig. 4.13 The piezoelectric current output and the definition of response time and the slope of the positive output currents.

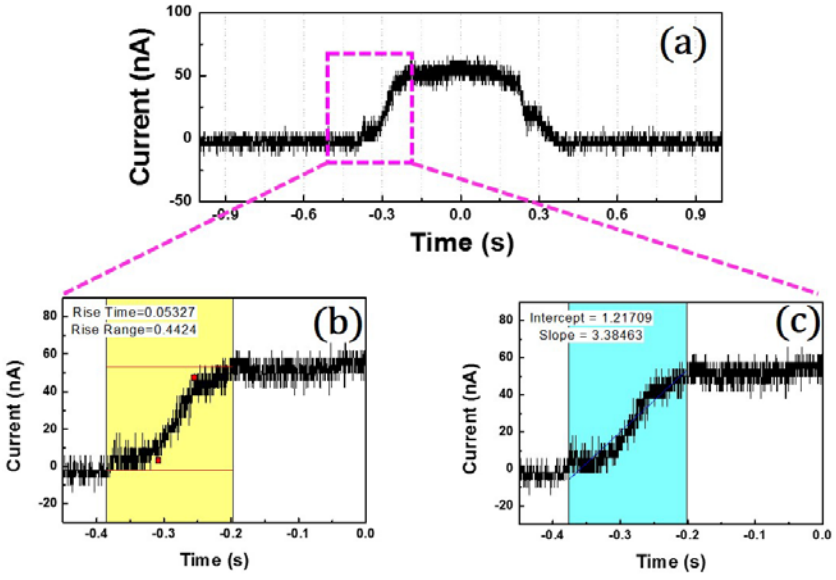

Fig. 4.14 The pyroelectric current output and the definition of response time and the slope.

The set of piezo-pyro electric current output signal is shown in Fig. 4.13 and Fig. 4.14 respectively. When we assume that the piezo and pyro electric output signal is collected from the cell arrays, the positive peak of piezoelectric signal and pyroelectric peak may be confused. The differentiation of two peaks is required for analyzing the signals. In Fig. 4.13, the enlarged positive single peak is presented. The response time of the positive peak is the rise time from the 10 % of electric output value to the 90 % of the peak level. And the slope of the positive peak is presented from the ground level to the peak value. The pyroelectric signal is also presented with the same definition of piezoelectric signal as shown in Fig. 4.14. Set of piezo-pyro electric signals are analyzed. The response time and the slope of selective piezoelectric output current signals which have current values in the similar range with the pyroelectric current values are compared with the pyroelectric current outputs. As shown in Fig. 4.15, the plots of both signals are in the same range. Therefore, comparison of the response time and slope of peaks are not suitable for verifying the piezo and pyroelectric output signals.

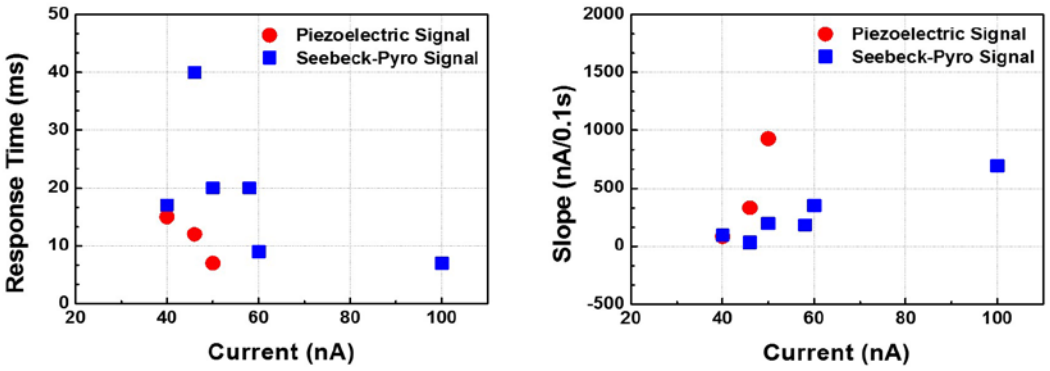

Fig. 4.15 The response time and the first slope of positive peaks of piezo-pyro electric current outputs. The blue squares correspond to the pyroelectric signals and the red circles correspond to the piezoelectric current outputs which have similar current level with pyroelectric current levels.

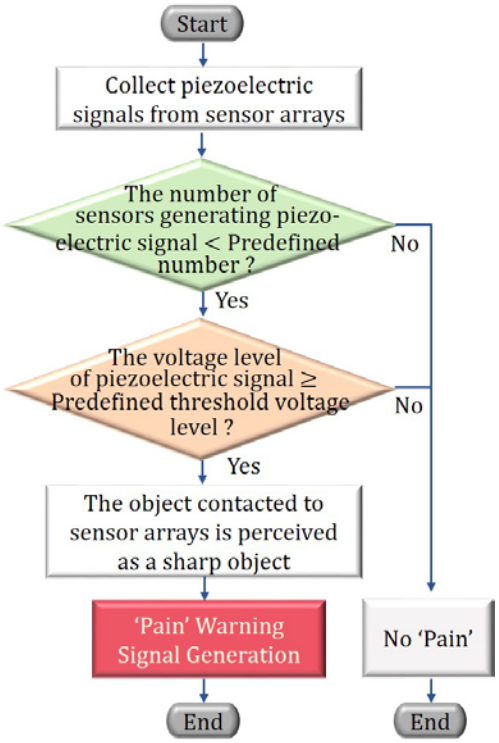

Fig. 4.16 Flow chart of signal processing generating 'pain' warning signals.

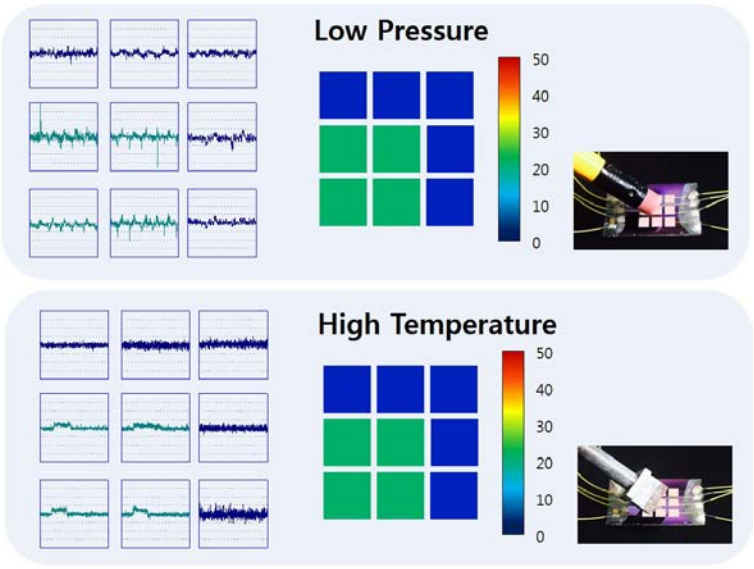

Fig. 4.17 Visual images of piezoelectric voltages generated by an eraser and a soldering iron.

The same visual images are presented even though the object touched the sensors are different.

Fig. 4.16 shows the flow chart of signal processing that generates 'pain' warning

signal. First of all, the ‘pain’ warning signal generation is demonstrated without hot-warning signal generation. The tactile sensor collects piezoelectric signals from sensor arrays. Then, the number of piezoelectric signal generating is checked. If the number of sensor generating

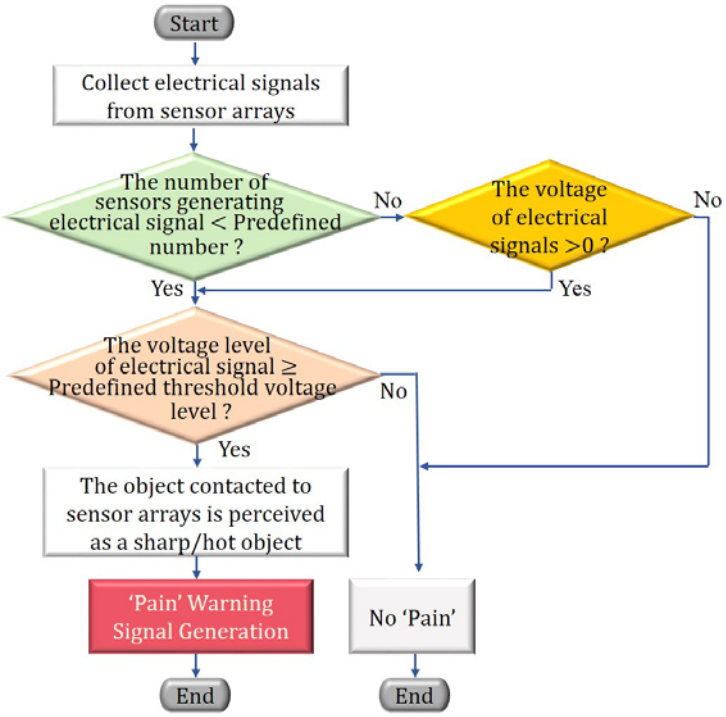

Fig. 4.18 Flow chart of signal processing generating ‘pain’ warning signals with an added step.

piezoelectric signal is more than the number of predefined number of sensor, the object touched sensor is considered to be blunt that does not generate ‘pain’ warning signal. If not, the voltage level of piezoelectric signal should be analyzed if the signal output level is higher than the predefined voltage threshold level or not. The object contacted to the sensor array is perceived as a sharp object when the piezoelectric output signal is higher than the ‘pain’ off-set. If the hot object touched the sensor in broad area of sensor arrays, this flow chart could not generate ‘pain’ warning signal because the threshold of pyroelectric signal is a lot lower than the threshold of piezoelectric output signal. As shown in Fig. 4.17, when the hot object such as soldering iron touched the sensor, the system perceives the signal patterns as the

blunt object due to the number of the sensor generating signals. Thus, another mechanism is desired to detect hot ‘pain’ feeling.

In order to add the ability to generate hot ‘pain’ warning signal to this system, one more step is required to be added on the original flow chart as shown in Fig. 4.18. The hot ‘pain’ warning signals are generated due to the temperature increasing and the positive peak is generated. Otherwise, the high pressure ‘pain’ piezoelectric signal is observed as negative peak for the first time. After the step checking the number of sensor generating piezoelectric signal, there may be the pyroelectric signals filtered as ‘no-pain’ signals because the pyroelectric signals could be generated from the many sensor arrays as like the blunt object touched the sensor arrays. The collected signals should be checked again by collecting positive peak signals because the hot ‘pain’ can be generated in broad range of sensor arrays. Then, the positive peak output signal level is compared with the predefined ‘pain’ threshold. Even though the peak is generated in the large number of arrays, the hot ‘pain’ warning signal is generated with this algorithm. However, when we think about the system collecting the piezo-pyro electric signals from the arrays, it could not verify the origin of the peaks. Random signals are collected from the arrays and the analysis of signals is impossible. Thus, for the real-time analysis of piezo and pyroelectric signals, revision of flow chart is required.

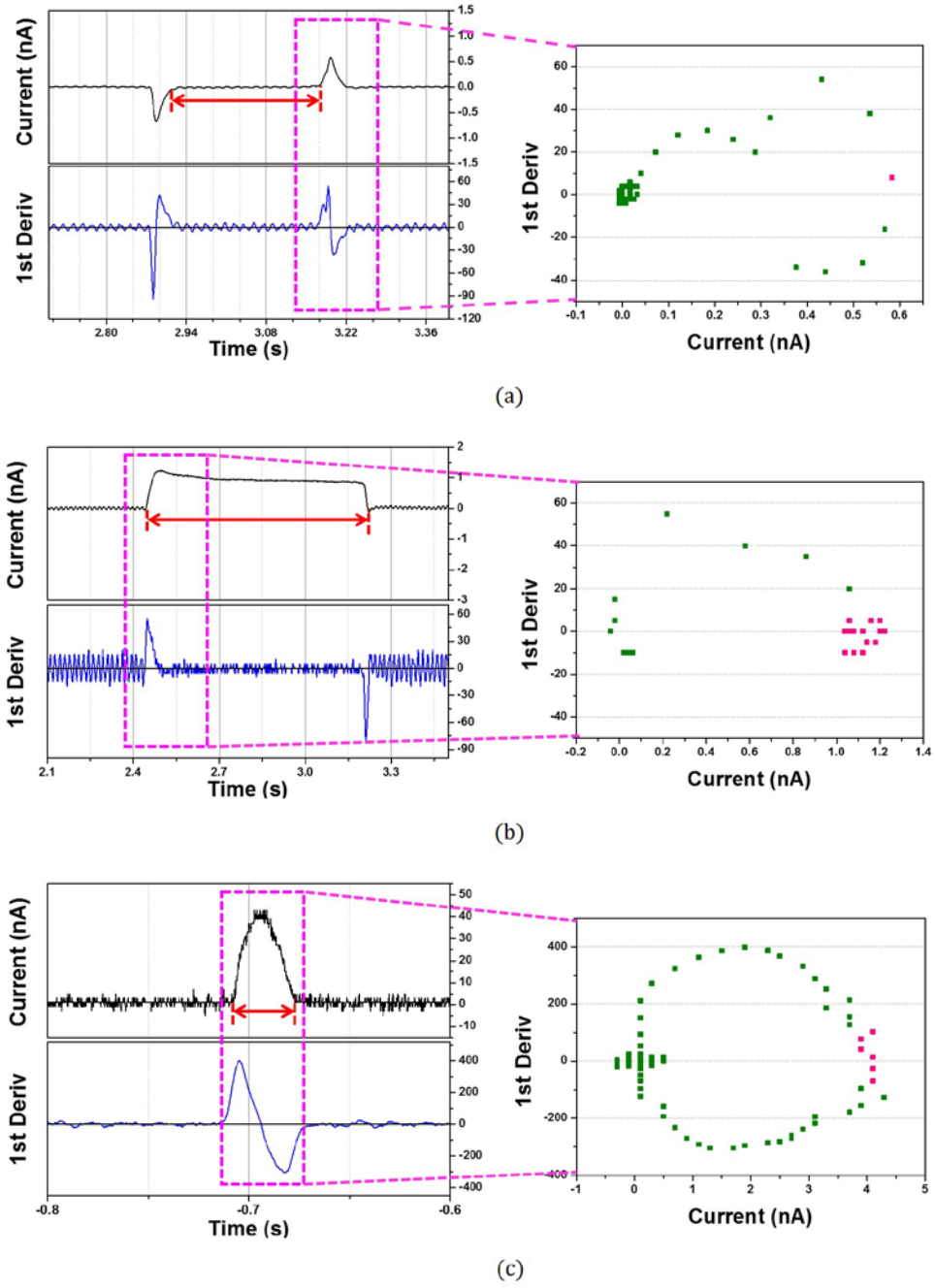

Fig. 4.19 The piezo-pyro electric signals and the plots of 1st derivatives–currents. (a) The piezoelectric current signal and the 1st derivatives-currents plot in the pink box, (b)The pyroelectric current signal, (c) The pyroelectric signal when the hot objet touched the sensor as fast as possible and the 1st derivatives-current plot in the pink boxes.

Fig. 4.19 (a) shows a set of pressure signals of one cell in arrays when the object

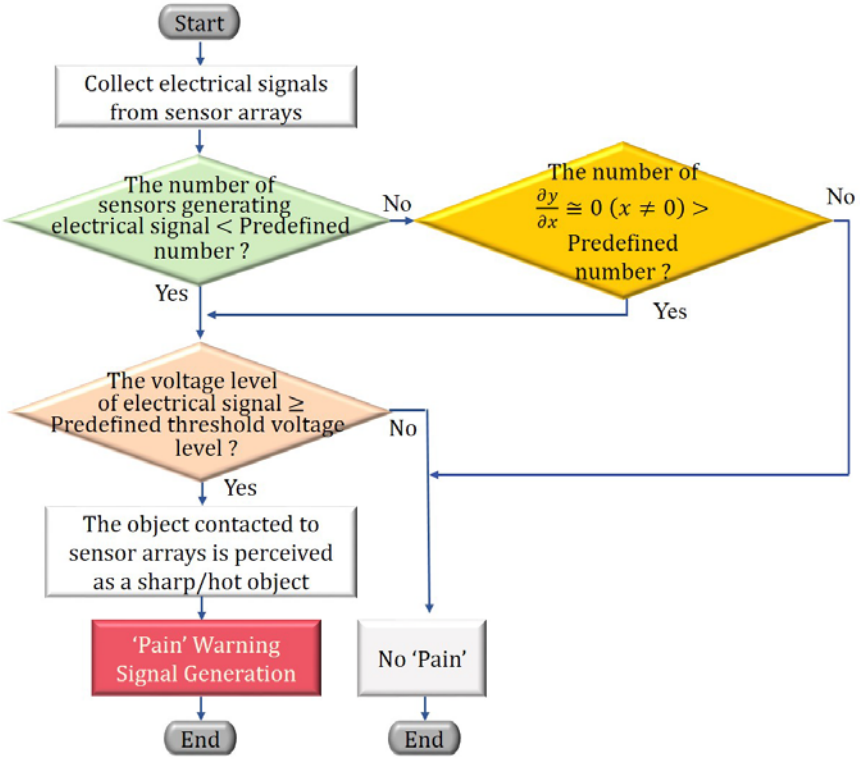

Fig. 4.20 Final flow chart of signal processing generating 'pain' warning signals.

touched the sensor. Fig. 4.19 (b), (c) shows the temperature output signal when the hot object activated the cell in tactile sensor. Fig. 4.19 (c) indicates that the touching signal of hot object in extreme short time which resembles the releasing piezoelectric signal. Therefore, it does not seem to be simply differentiated between them. Fig. 4.19 shows current-1st derivatives curves of each part of the pink boxes. When we focused on the point where the 1st derivatives are zero, there are big differences between pressure and temperature signals. The number of the spots in pressure signals where the 1st derivatives got zero is lower than that of temperature signals. This implies that the saturation time of the pressure signal is a lot shorter than that of the temperature signal. Then, we can set the criteria of the signals in which we can say one is the pressure signal or temperature signal. Fig. 4.20 shows the final signal processing algorithm for the high pressure and temperature 'pain' warning signal generation system. The collection of piezo-pyro electric signals is conducted and then the number of the

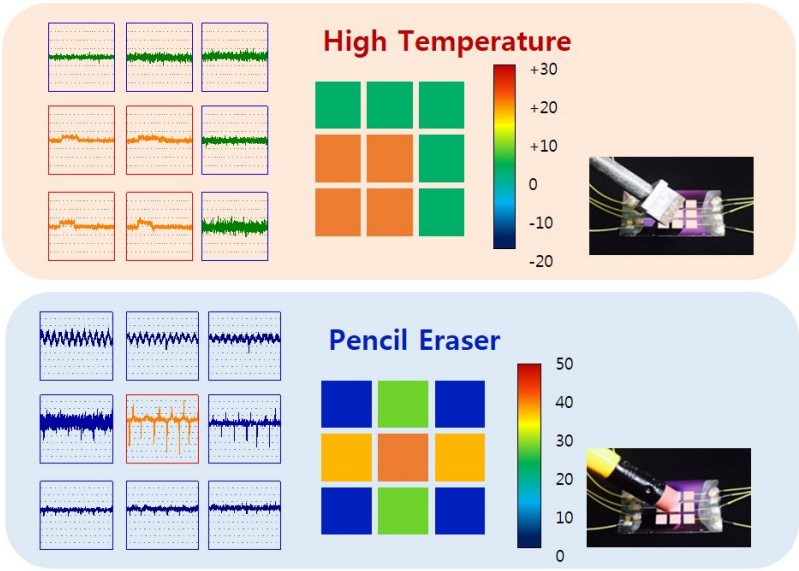

Fig. 4.21 Visual images of piezoelectric voltages generated by an eraser and a soldering iron. The differentiation between blunt object and the hot object touching the sensors.

sensors generating electrical output signal is compared with the predefined number of the sensors. The signals generated in small amount of sensors, the output electrical signal level need to be checked if the level is higher than the 'pain' offset. At the same time, among the filtered signals from previous step, the number of values that have $\frac{\partial y}{\partial x} = 0$ is analyzed from the current-1st derivatives plots. If the number of values that have $\frac{\partial y}{\partial x} = 0$ is more than the predefined numbers, the peak is considered to be pyroelectric output signal. Then, the signals proceeded to the next steps for checking the 'pain' warning signals. Therefore, the hot 'pain' warning and the high pressure 'pain' warning signal generation are possible with the final flow chart. When the high temperature input is induced to the sensor even in the broad area, the system could generate hot 'pain' warning signal (Fig. 4.21).

V. **CONCLUSION**

We have demonstrated the tactile sensor which can produce psychological feelings. The most important feeling for humans to interact with external environments is the ‘pain’ feeling. The ZnO nanowire is a good candidate for the ‘pain’ warning signal generation which derived from high pressure and high temperature inputs. By utilizing the piezo-pyro electric effects and Seebeck currents inside of the ZnO nanowires, we successfully demonstrated ‘pain’ warning signal generating system. The array type of tactile sensor is fabricated from the concept of human tactile sensing system. Also, the algorithm for the differentiation of piezo and pyro-Seebeck outputs is suggested. The various electrical outputs are measured according to the input scenarios: 1) Low (High) pressure; 2) Low (High) temperature; 3) Low (High) pressure with Low (High) temperature. From the random electrical signals, we can easily separate ‘pain’ and ‘no-pain’ signals. The distribution of sensor arrays which generate electrical signals and the output voltage/current level are criteria for the ‘pain’ warning signal generation. The hot ‘pain’ warning signal generation depends on the shape of electrical output signals. The 1^{st} derivatives of the piezo-pyro electric outputs are the key factors for the detection of hot ‘pain’ feelings. Therefore, three of statuses: high pressure, high temperature and softness can be differentiated. In order to develop the advanced tactile sensors, the high sensitive pressure/temperature sensor is necessary and more parameters should be integrated in tactile sensor such as shear, force and strain. This capability enables that the tactile sensor can convey psychological feelings as like human from several physical parameters. Ultimately, this tactile sensor is expected to be utilized to protect android robot hands or mobile phone touch displays from external harsh environments.

References

[1] Dahiya, R. S., Metta, G., Valle, M., & Sandini, G. (2010). "Tactile sensing—from humans to humanoids." *Robotics, IEEE Transactions on*, *26*(1), pp. 1-20.

[2] Yousef, H., Boukallel, M., & Althoefer, K. (2011). "Tactile sensing for dexterous in-hand manipulation in robotics—A review." *Sensors and Actuators A: physical*, *167*(2), pp. 171-187.

[3] Girão, P. S., Ramos, P. M. P., Postolache, O., & Pereira, J. M. D. (2013). "Tactile sensors for robotic applications." *Measurement*, *46*(3), pp. 1257-1271.

[4] Chun, J., Lee, K. Y., Kang, C. Y., Kim, M. W., Kim, S. W., & Baik, J. M. (2014). "Embossed Hollow Hemisphere-Based Piezoelectric Nanogenerator and Highly Responsive Pressure Sensor." *Advanced Functional Materials*, *24*(14), pp. 2038-2043.

[5] Pang, C., Lee, G. Y., Kim, T. I., Kim, S. M., Kim, H. N., Ahn, S. H., & Suh, K. Y. (2012). "A flexible and highly sensitive strain-gauge sensor using reversible interlocking of nanofibres." *Nature materials*, *11*(9), pp. 795-801.

[6] Shih, W. P., Tsao, L. C., Lee, C. W., Cheng, M. Y., Chang, C., Yang, Y. J., & Fan, K. C. (2010). "Flexible temperature sensor array based on a graphite-polydimethylsiloxane composite." *Sensors*, *10*(4), pp. 3597-3610.

[7] Yamada, D., Maeno, T., & Yamada, Y. (2001). "Artificial finger skin having ridges and distributed tactile sensors used for grasp force control." In *Intelligent Robots and Systems, 2001. Proceedings. 2001 IEEE/RSJ International Conference on* (Vol. 2, pp. 686-691). IEEE.

[8] Lippiello, V., Ruggiero, F., Siciliano, B., & Villani, L. (2013). "Visual grasp planning for unknown objects using a multifingered robotic hand." *Mechatronics, IEEE/ASME Transactions on*, *18*(3), pp. 1050-1059.

[9] Xu, S., Qin, Y., Xu, C., Wei, Y., Yang, R., & Wang, Z. L. (2010). "Self-powered nanowire devices." *Nature nanotechnology*, *5*(5), pp. 366-373.

[10] Yang, Y., Zhou, Y., Wu, J. M., & Wang, Z. L. (2012). "Single micro/nanowire pyroelectric nanogenerators as self-powered temperature sensors." *ACS nano*, *6*(9), pp. 8456-8461.

[11] Yang, Y., Jung, J. H., Yun, B. K., Zhang, F., Pradel, K. C., Guo, W., & Wang, Z. L. (2012). "Flexible Pyroelectric Nanogenerators using a Composite Structure of Lead-Free KNbO3 Nanowires." *Advanced Materials*, *24*(39), pp. 5357-5362.

[12] Yang, Y. et al. (2012). "Pyroelectric nanogenerators for harvesting thermoelectric energy." *Nano letters*, *12*(6), pp. 2833-2838.

[13] Lee, J. H. et al. (2014). "Highly Stretchable Piezoelectric-Pyroelectric Hybrid Nanogenerator." *Advanced Materials*, *26*(5), pp. 765-769.

[14] Johansson, R. S., & Westling, G. (1984). "Roles of glabrous skin receptors and sensorimotor memory in automatic control of precision grip when lifting rougher or more slippery objects." *Experimental brain re-*

search, *56*(3), pp. 550-564.

[15] Johansson, R. S., & Vallbo, Å. B. (1979). “Tactile sensibility in the human hand: relative and absolute densities of four types of mechanoreceptive units in glabrous skin.” *The Journal of physiology*, *286*(1), pp. 283-300.

[16] Athenstaedt, H., Claussen, H., & Schaper, D. (1982). “Epidermis of human skin: pyroelectric and piezoelectric sensor layer.” *Science*, *216*(4549), pp. 1018-1020.

[17] C. Craig, Jayne M. Kisner, J. (1998). “Factors affecting tactile spatial acuity.” *Somatosensory & motor research*, *15*(1), pp. 29-45.

[18] Goldstein, E. (2013). *Sensation and perception*. Cengage Learning, vol. 9, 496 pages

[19] S. J. Lederman. (1978). “Heightening tactile impressions of surface texture,” in Active Touch: The Mechanicsm of Recognition of Objects by Manipulation. An Interdisciplinary Approach, G. Gordon, Ed. Oxford, U.K.: Pergamon, pp. 205–214.

[20] R. L. Klatzky and S. J. Lederman. (2003). *Touch, Handbook of Psychology*. New York: Wiley, vol. 4, pp. 147–176.

[21] J. C. Craig and X. Baihua. (1990). “Temporal order and tactile patterns,” Percept. Phychophys., vol. 47, no. 1, pp. 22–34.

[22] L. A. Jones and S. J. Lederman. (2006). “Tactile sensing,” in Human Hand Function. Cambridge, MA: Oxford Univ. Press, pp. 44–74.

[23] J. C. Stevens and K. K. Choo. (1998). “Temperature sensitivity of the body surface over the life span,” Somatosens. Motor Res., vol. 15, pp. 13–28.

[24] Tiwana, M. I., Redmond, S. J., & Lovell, N. H. (2012). “A review of tactile sensing technologies with applications in biomedical engineering.” *Sensors and Actuators A: physical*, *179*, pp. 17-31.

[25] Silvera-Tawil, D., Rye, D., & Velonaki, M. (2015). “Artificial skin and tactile sensing for socially interactive robots: A review.” *Robotics and Autonomous Systems*, *63*, pp. 230-243.

[26] Zhang, H., & So, E. (2002). “Hybrid resistive tactile sensing.” *Systems, Man, and Cybernetics, Part B: Cybernetics, IEEE Transactions on*, *32*(1), pp. 57-65.

[27] Pang, C., Lee, G. Y., Kim, T. I., Kim, S. M., Kim, H. N., Ahn, S. H., & Suh, K. Y. (2012). “A flexible and highly sensitive strain-gauge sensor using reversible interlocking of nanofibres.” *Nature materials*, *11*(9), pp. 795-801.

[28] Lee, H. K., Chung, J., Chang, S. I., & Yoon, E. (2011). “Real-time measurement of the three-axis contact force distribution using a flexible capacitive polymer tactile sensor.” *Journal of Micromechanics and Microengineering*, *21*(3), 035010.

[29] Kim, S. Y., Park, S., Park, H. W., Park, D. H., Jeong, Y., & Kim, D. H. (2015). “Highly Sensitive and Multimodal All-Carbon Skin Sensors Capable of Simultaneously Detecting Tactile and Biological Stimuli.” *Advanced Materials*, *27*(28), pp. 4178-4185.

[30] Yun, S., Park, S., Park, B., Kim, Y., Park, S. K., Nam, S., & Kyung, K. U. (2014). “Polymer-Waveguide-Based Flexible Tactile Sensor Array for Dynamic Response.” *Advanced Materials*, *26*(26), pp. 4474-4480.
[31] Ando, S., & Shinoda, H. (1995). “Ultrasonic emission tactile sensing.” *Control Systems, IEEE*, *15*(1), pp. 61-69.

[32] E. Torres-Jara, I. Vasilescu, and R. Coral. (2006). “A soft touch: Compliant tactile sensors for sensitive manipulation,” CSAIL, Mass. Inst. Technol., Cambridge, MA, Tech. Rep. MIT-CSAIL-TR-2006-014.

[33] Wang, Z. L., & Song, J. (2006). “Piezoelectric nanogenerators based on zinc oxide nanowire arrays.” *Science*, *312*(5771), pp. 242-246.

[34] Tichý, J., Erhart, J., Kittinger, E., & Prívratská, J. (2010). *Fundamentals of piezoelectric sensorics: mechanical, dielectric, and thermodynamical properties of piezoelectric materials*. Springer Science & Business Media, 207 pages.

[35] Walker, G. (2012). “A review of technologies for sensing contact location on the surface of a display.” *Journal of the Society for Information Display*, *20*(8), pp. 413-440.

[36] Jeong, Y. et al., (2015). “Psychological tactile sensor structure based on piezoelectric nanowire cell arrays.” *RSC Advances*, *5*(50), pp. 40363-40368.

[37] Cha, S et al., (2011). “Porous PVDF as effective sonic wave driven nanogenerators.” *Nano letters*, *11*(12), pp. 5142-5147.

[38] Wang, Z. L. (2009). “ZnO nanowire and nanobelt platform for nanotechnology.” *Materials Science and Engineering: R: Reports*, *64*(3), pp. 33-71.

[39] Kasap, S.O. (2006). *Principles of electronic materials and devices*. McGraw-Hill, vol. 3, 874 pages.

요 약 문

ZnO 나노와이어를 이용한 압력과 온도 센서 개발

최근 사람의 촉각 시스템을 모방하는 촉각 센서 연구가 활발히 진행되고 있다. 하지만 이러한 촉각 센서들은 단순히 압력이나 압력의 분포만을 인지하거나 압력이나 온도 측정의 민감도를 향상하는 방향으로 연구되고 있고, 특히 로봇공학에서는 로봇 손의 그립 제어를 통한 달걀과 같은 깨지기 쉬운 물체를 잡는 것에 초점을 맞추어 촉각센서가 개발되고 있다. 사람에게는 부드러움, 거침, 고통과 같은 정신 감각적인 느낌이 다른 사람과 물체와 교감하는 데 중요한 요소 중 하나이다. 만약 촉각센서가 정신 감각적인 느낌을 제공할 수 있다면, 이러한 촉각 센서가 적용된 로봇 손, 의수 또는 디스플레이는 사람과 같이 정신 감각적인 느낌을 제공하거나 느낄 수 있게 되어 가혹한 환경으로부터의 보호, 사람의 감정을 제공하는 디바이스의 개발 등 그 응용 분야가 무궁무진하다. 정신 감각적인 느낌 중에서 고통은 가장 중요한 요소로서 사람이 외부 환경으로부터 위험을 감지하고 자기방어를 가능하게 한다. 궁극적으로, 사람과 같이 지능적인 로봇은 위험을 감지함과 동시에 그 상황에서 탈출을 동시에 수행하는 것이 가능하다. 이러한 관점에서 고통을 느끼는 촉각 센서의 개발은 필수적이나 현재까지 진행된 연구가 부족하다. 고통을 유발하는 물리적인 인자는 압력과 온도라는 점에 착안하여 본 연구에서는 ZnO 나노와이어의 특성을 이용하였다. ZnO 나노와이어의 압전, 초전 효과를 이용하여 압력과 온도를 센싱할 수 있으며 자가발전, 멀티터치가 가능한 촉각센서의 개발이 가능하다. 또한, 플렉서블 디바이스로 구현하기 위해서는 저온 공정이 필수적인데 ZnO 나노와이어의 수열 합성을 통한 센서 제작은 저온공정이 보장되는 장점이 있다. 본 연구에서는 사람 피부의 변형을 모방하는 센서를 구현하기 위해 3 × 3 어레이 타입의 센서를 구현하여 온도와 압력에 대한 신호를 구별할 수 있는 신호처리 방법을 고안하였다. 간단한 신호처리 기법을 통해 온도와 압력에 대한 신호를 구별하여 고통을 인지하는 센서를 구현할 수 있으며 압력, 온도, 압력과 온도의 동시 신호 등 여러 가지 입력에 대한 신호를 구별하는 것이 가능하다. 본 연구는 기존의 단순한 물리적인 값을 측정하는 온도와 압력 센서와 달리 전기 기계적 방법을 통한 정신 감각적 느낌 중 하나인 고통을 느끼는 센서를 직관적이고 단순한 디자인을 통해 구현하였다는 점에서 그 의의를 가진다.

핵심어: 촉각센서, ZnO 나노와이어, 온도&압력 센서

Acknowledgements

Though this dissertation is an individual work, I could never have reached the heights or explored the depths without help, support, guidance and efforts of a lot of people. First and foremost, I would like to thank my advisor, Prof. Jae Eun Jang, for his unstinted support throughout my research. He has not only given a number of advice, but also taken time to patiently discuss every details of the work. He has provided me opportunities to open my eyes to my research area and has supported me in every manner.

I would like to thank my committee members Prof. Seong-Woon Yu and Prof. Ji-Woong Choi for their guidance over the years. I would also like to thank faculty members of department of Information and Communication Engineering at DGIST; Prof. Wook Hyoun Kwon, Prof. Sang Hyuk Son, Prof. Yongsoon Eun, Prof. Minkyu Je, Prof. Jihwan Choi, Prof. Jae Youn Hwang, Prof. Min-Soo Kim, Prof. Kyung-Joon Park. They have usually provided me a lot of opportunities to enhance my academic knowledge and techniques.

Thanks also go to lab members of AEDRG; Jeong Hee Shin, Gwang Jun Lee, Byoung-Ok Jun, Seunguk Kim, Jae Hoon Yang, Minkyung Sim, Mingyu Ryu, Young Jin Lee and Kwon Sik Shin. They have always encouraged me to finish this work and given advice regarding all the techniques and skills for this work.

Last but not least, I would like to thank my family and friends supporting with limitless love for me to complete the graduate program. I would not have been able to complete this thesis without their continuous love and encouragement.